RESEARCH ARTICLE

Higher levels of kallikrein-8 in female brain may increase the risk for Alzheimer's disease

Kathy Keyvani[1]; Yvonne Münster[1]; Nirup K. Kurapati[1]; Sebastian Rubach[1]; Andreas Schönborn[1];
Emre Kocakavuk[1]; Mohamed Karout[1]; Pia Hammesfahr[1]; Ya-Chao Wang[2]; Dirk M. Hermann[2];
Sarah Teuber-Hanselmann[1]; Arne Herring [iD][1]

[1] Institute of Neuropathology, [2] Department of Neurology, University of Duisburg-Essen, Hufelandstr. 55, 45122 Essen, Germany.

Abstract

Women seem to have a higher vulnerability to Alzheimer's disease (AD), but the underlying mechanisms of this sex dichotomy are not well understood. Here, we first determined the influence of sex on various aspects of Alzheimer's pathology in transgenic CRND8 mice. We demonstrate that beta-amyloid (Aβ) plaque burden starts to be more severe around P180 (moderate disease stage) in female transgenics when compared to males and that aging aggravates this sex-specific difference. Furthermore, we show that female transgenics suffer from higher levels of neurovascular dysfunction around P180, resulting in impaired Aβ peptide clearance across the blood-brain-barrier at P360. Female transgenics show also higher levels of diffuse microgliosis and inflammation, but the density of microglial cells surrounding Aβ plaques is less in females. In line with this finding, testosterone compared to estradiol was able to improve microglial viability and Aβ clearance *in vitro*. The spatial memory of transgenics was in general poorer than in wildtypes and at P360 worse in females irrespective of their genotype. This difference was accompanied by a slightly diminished dendritic complexity in females. While all the above-named sex-differences emerged after the onset of Aβ pathology, kallikrein-8 (KLK8) protease levels were, as an exception, higher in female than in male brains very early when virtually no plaques were detectable. In a second step, we quantified cerebral KLK8 levels in AD patients and healthy controls, and could ascertain, similar to mice, higher KLK8 levels not only in AD-affected but also in healthy brains of women. Accordingly, we could demonstrate that estradiol but not testosterone induces KLK8 synthesis in neuronal and microglial cells. In conclusion, multiple features of AD are more pronounced in females. Here, we show for the first time that this sex-specific difference may be meditated by estrogen-induced KLK8 overproduction long before AD pathology emerges.

INTRODUCTION

Alzheimer's disease is the most common neurodegenerative disease and the primary cause for dementia. It is now recognized that gender is a strong contributor to disease vulnerability. Women have a higher prevalence for Alzheimer's disease, accounting for almost two-thirds of all patients (8). Even though this might be partially explained by increased premature mortality of men (beginning around 45 years), women aged 65 years and older are almost twice as likely to develop Alzheimer's disease compared with age-matched men (61). Furthermore, women are affected by a faster progression of mild cognitive impairments (40), show a higher transition rate from mild cognitive impairment to Alzheimer's disease after the age of 80 years (53) and suffer from a more pronounced severity for clinical dementia (31, 42, 47). Sex-differences in disease-related cognitive impairments and pathology burden can be

also detected in various transgenic mouse models of Alzheimer's disease, with female mice being more severely affected by cognitive deficits (14, 35, 49) and Aβ plaque pathology than males (9, 30, 37, 63).

Epidemiological and experimental studies indicate that multiple biological (sex differences) as well as sociocultural factors (gender differences, such as education or employment and further lifestyle factors like social activities and exercise) contribute to the diverging development and progression of Alzheimer's disease between women and men (42, 58).

Biological contributors can be of genetic, epigenetic or hormonal nature. For example, the *APOE ε4* gene is reported to increase the risk of Alzheimer's disease and to promote the conversion from mild cognitive impairment to Alzheimer's disease particularly in women (2, 20) and further to provoke cognitive deficits predominantly in female mice (51), whereas the neuroprotective potential

of the *APOE ε2* allele against Alzheimer's disease is greater in men than in women (2). Also sex hormones are probable modulators of disease susceptibility, although clinical trials in humans and animal experiments partially provide conflicting results. Estrogen seems to display neuroprotective functions (57) and counteracts Alzheimer's disease-related beta-amyloid (Aβ) and tau pathology in mice (48) but fails to benefit cognition in menopausal women undergoing hormonal replacement therapy (19, 23). *In vivo* or *in vitro* treatment with androgens also protects against Aβ pathology in non-human studies (46, 52) and age-related testosterone reduction seems to increase disease risk in humans (55). Inter-species discrepancies may arise from the fact that human aging is characterized by a relatively abrupt estradiol drop in women and a steady decrease of testosterone in men (6), whereas gonadal steroid hormone levels remain stable in aging mice (18).

Taken together, it seems very suggestive that physiological aging causes a microenvironment particularly in female brain that might promote Alzheimer's disease susceptibility (67), however the underlying mechanism of this discrimination is largely not understood. Even our descriptive knowledge about the ontogeny of sex-associated differences in Alzheimer's disease is very patchy.

In the present study, we systematically compared the effect of sex and aging on various aspects of Alzheimer's disease-related pathology, that is, Aβ and tau pathology, neurovascular dysfunction, neuroinflammation, memory impairments and agitation, as well as structural plasticity and autophagy deficits in transgenic CRNC8 mice (and age-matched healthy controls) covering several time points before disease onset thru a late disease stage. Additionally, as we could previously demonstrate an exceedingly early and multifocal excess of the protease kallikrein-8 (KLK8, also known as neuropsin) in Alzheimer's disease-affected and scarcely-affected human and murine brain areas (such as hippocampus, frontal cortex, entorhinal cortex and cerebellum) even before disease onset and as we could show multiple therapeutic effects of KLK8 inhibition on Alzheimer's pathology in mice (ie, reduced Aβ and tau pathology, improved neurovascular function, autophagy and neuroplasticity resulting in enhanced cognitive function and diminished anxiety-like behavior) (28), we now examined whether there are any sex-dependent effects on cerebral KLK8 expression, and if so, whether these differences might play a causal role in the context of disease-related female/male dichotomy.

MATERIALS AND METHODS

General

All results were generated in blind-coded experiments, in which the person who collected the data was unaware of the specific murine genotype and sex or the human health status and sex. Protein, peptide and mRNA levels were quantified individually in duplicates or triplicates in separate brain areas.

Experimental animals

Female and male TgCRND8 mice (TG, hemizygously carrying and over-expressing a double-mutant human APP 695 transgene [*hAPP*+/−] harboring the "Swedish" and "Indiana" mutations [KM670/671NL & V717F] under the control of the hamster Prion

protein promoter on a C57BL/6-C3H/HeJ hybrid background strain) as well as female and male wildtype (WT, C57BL/6-C3H/HeJ hybrid background) littermates were used. Transgenic mice are characterized by early stereotypic behavior starting at 2 months of postnatal age (P60) (4), followed by cerebral Aβ plaque formation with simultaneous cognitive impairment (at approx. P90) (11). Mice from both genotypes and sexes were kept in standard housing (SH) cages (Makrolon type III) together with their dams until either P3 (early postnatal period, n = 6 per genotype and sex) or P30 (early juvenile period, before the onset of Aβ pathology, TG female n = 8, TG male n = 6, WT n = 4 per sex). Additional litters were housed together with their dams until P30 and then transferred to single-sex groups of 3–4 in SH cages until P90 (around disease onset), P180 (moderate disease stage) or P365 (late disease stage) (n = 4–12 per genotype, sex and age). To minimize a biased effect of the parental genotype on the phenotype of the investigated mice, equal numbers of female and male transgenic and wildtype mice per litter were assigned to different groups.

Behavioral phenotyping

Transgenic and wildtype female and male mice were behaviorally phenotyped between P366 and P371. Prior to testing, all animals had been adapted to an inverted day/night cycle for 1 week. First, mice were tested in the Open Field (OF) for exploratory behavior and general activity according to (34) at P366. The OF arena (52 × 52 × 30 cm) was located 72 cm above the floor on a circular platform. Each mouse was placed near the wall and observed for 10 minutes. The test arena was divided into one center (31.2 × 31.2 cm), four border (each 10.4 × 31.2 cm) and four corner (each 10.4 × 10.4 cm) areas. Number of entries, latencies until first time entries, duration and distance covered in each area as well as velocity were automatically recorded and analyzed by Video Mot 3D software (TSE, version 7.0.1). Afterwards, hippocampus-associated spatial memory and learning performance was assessed by the Barnes Maze (BM) according to (59) from P367 until P371. The BM arena was composed of a circular platform (92 cm diameter, 120 cm above the ground) with 20 equally distributed holes (5-cm diameter, 7.5-cm distance between holes) located at the border. One hole (escape hole) was connected to a box (15.5 × 9.5 × 6 cm), allowing to escape from the BM platform, whereas the other 19 holes were not connected to the escape box (error holes). Twenty-four hours before tests started, mice were habituated to the setup for two trials, each lasting for 3 minutes. Tests were performed between 10:00 am and 6:00 pm. Each mouse was placed in a black cylinder located in the middle of the platform for 10 s. Meanwhile, red light was switched to bright light (180 lx) and the cylinder was lifted, defining the start of a 3-minute trial. During each trial, primary errors, total errors, primary latency, total latency, path length covered and velocity were automatically determined. Primary errors and latencies were defined as the number and duration of approximations to error holes until approaching the escape hole for the first time. Total errors and latencies were defined as the number and duration of approximations to error holes and to the escape hole until final escape. Once a mouse escaped, it was allowed to stay in the escape box for 1 minute before being transferred to the home cage. If a mouse did not escape during the 3-minute interval, it was gently guided to the escape hole until the mouse

escaped; otherwise it was placed directly into the escape box for 1 minutes. On test day 1, each mouse was tested in four trials. On test days 2, 3, 4 and 5, each mouse was tested in two trials. Inter-trial intervals lasted for 15 minutes. Following the four test days, the escape hole and the error holes were blocked at day 5 (probe trial). Mice were allowed to explore the platform for 90 s per probe trial. Before and after each test, the OF and BM arenas were cleaned with 70% ethanol.

Murine blood and tissue sampling

Young and adult mice from both genotypes and sexes were sacrificed (in deep anesthesia) at P3, P30, P90 or P187 (consecutively designated as P180), respectively. Neocortex, hippocampus and basal ganglia were isolated and separately homogenized from one hemisphere. Homogenates were subjected to DNA, RNA and protein extraction (15596-018, TRIzol-reagent, life technologies). The other hemisphere was formalin-fixed, paraffin embedded and cut into 10 µm coronal sections for immunohistochemistry.

From old transgenics, blood was collected at P372 (one day after the final BM test day, consecutively designated as P360) from retrobulbar venous plexus to determine baseline circulating plasma Aβ levels (time: 0 minute = t_0). To quantify Aβ efflux efficacy across the blood-brain-barrier (BBB), an Aβ stabilizing anti-Aβ antibody [HJ5.1, 150 µg/animal, purchased from Dr. David M. Holtzman's lab, St. Louis, Missouri (10), enters brain parenchyma only marginally, does not influence the Aβ-brain-to-blood-equilibrium, and protects Aβ from enzymatic fragmentation] was intravenously injected (via the tail vein) into transgenic mice to prevent the naturally occurring rapid Aβ degradation in blood ($t_{1/2}$ = 2–3 minutes) which precludes a direct and sensitive quantification of brain-derived Aβ over baseline circulating plasma Aβ. Two transgenics received saline as control. Ten and forty minutes after HJ5.1-antibody or saline injection blood was sampled again (t_{10} and t_{40}). Intravenous anti-Aβ antibody injection and retrobulbar venous blood collection was performed in anesthetized mice with 2% isoflurane in oxygen/nitrous oxide (20%:40%). Immediately after blood collection, transgenic and wildtype mice were sacrificed (in deep anesthesia). Neocortex, hippocampus and basal ganglia were isolated from one hemisphere and subjected to DNA, RNA and protein extraction in analogy to brain preparation from young and adult mice. Additionally, the frontal pole (+4 to +1.5 Bregma) from the other intact hemisphere was treated with Golgi-Cox solution (PK401-A, FD Rapid GolgiStain Kit, FD NeuroTechnologies) and subsequently cut into 200 µm coronal sections. The rest of the brain hemisphere was formalin-fixed, paraffin embedded and cut into 10 µm coronal sections for immunohistochemistry.

Human tissue sampling

Frozen hippocampi from Alzheimer's disease patients classified (by two neuropathologists) as CERAD (43) A/Braak and Braak (7) I-II (female: n = 7, age 69.86 ± 2.85 years, post-mortem interval (PMI) 34.57 ± 4.5 h; male: n = 6, age 69.17 ± 4.6 years, PMI 37.17 ± 5.77 h), CERAD B/Braak and Braak III-IV (female: n = 6, age 83 ± 2.21 years, PMI 26.82 ± 5.56 h; male: n = 7, age 73 ± 2.61 years, PMI 54.71 ± 14.41 h), CERAD C/Braak and Braak V-VI (female: n = 5, age 78.2 ± 3.86 years, PMI 64.25 ± 15.95 h; male: n = 6, age 74.33 ± 1.33 years, PMI

22.25 ± 6.66 h) as well as from neurologically healthy age-matched controls (female: n = 10, age 68.5 ± 2.64 years, PMI 39.3 ± 9.5 h; male: n = 13, age 69.15 ± 1.79 years, PMI 53.92 ± 9.26 h) were separately isolated and subjected to protein extraction using protein extraction buffer (containing 50 mmol/L Tris-HCl, pH 8.0, 150 mmol/L NaCl, 5 mmol/L EDTA, 10 mL/L NP-40, 0.5% proteinase inhibitor cocktail, Sigma P8340) for ELISA analyses or by TRIzol for immunoblotting analyses. A list of all human samples is available in Supporting Information Table S1.

Immunoblotting

Amyloid precursor protein (APP, and the C-terminal processing fragment CTFβ, 1:2000, A8717, Sigma-Aldrich), total protein levels of tau (1:500, tau-5, MAB361, Millipore), phospho-Ser202/Thr205-tau (AT8, 1:500, MN1020, Thermo Scientific), allograft inflammatory factor 1 (AIF1, 1:1500, AP08912PU-N, Acris), prostaglandin E receptor 2 (PTGER2, 1:500, AP01201PU-N, Acris), tumor necrosis factor alpha (TNFα, 1:1000, ab6671, abcam), triggering receptor expressed on myeloid cells 2 (TREM2, 1:500, ABIN749678, antibodies-online.com), synaptophysin (SYP, 1:10 000, M7315, DAKO), growth associated protein 43 (GAP43, 1:4000, GTX11136, GeneTex), activity regulated cytoskeletal-associated protein (ARC, 1:500, sc-15325, Santa Cruz Biotechnology), multidrug resistance protein 1B (MDR1, 1:1000, TA319318, Acris), clusterin (CLU, 1:750, ab92548, abcam), advanced glycosylation end product-specific receptor (RAGE, 1:1000, SP5151P, Acris), beclin-1 (1:2000, ab62557, abcam), autophagy related 5 (ATG5, 1:500, A0856, Sigma-Aldrich), syntaxin 17 (STX17, 1:1000, 17815-1-AP, Acris), kallikrein-8 (KLK8, 1:750, ABIN759116, antibodies-online.com) and fibronectin (1:1.000, ab2413, abcam) were quantified by immunoblot. Protein levels of glyceraldehyde-3-phosphate dehydrogenase (GAPDH, 1:15 000, G9545, Sigma-Aldrich) or determination of total protein load via fluorescent gel electrophoresis (TGX stain free gels, 161–0183, Bio-Rad) served for normalization.

Elisa

sAPPα (JP27734, IBL International), Aβ40 and Aβ42 (KHB3482 and KHB3442, Invitrogen) peptide levels were quantified by ELISA in murine protein extracts from cerebral homogenates containing 1% SDS. Aβ40 and Aβ42 were also determined in murine blood plasma via ELISA. Human KLK8 levels were measured using ELISA (EK0819, Boster) in hippocampal protein samples isolated with protein extraction buffer.

Quantitative real-time PCR

Transcription levels of *hAPP* were measured via quantitative real-time PCR (TaqMan assays, ABI 7500 Fast real-time PCR cycler, Applied Biosystems) following reverse transcription of DNase-treated RNA extracts to cDNA (ABI High-Capacity RT Kit, #4368814, Applied Biosystems) and normalized against *Gapdh* mRNA levels. Intron-spanning forward and reverse primer sequences and the TaqMan probe forward sequences are available on request.

Immunohistochemistry and quantification

Aβ plaques (6F/3D, 1:100, M0872, DAKO), microglia (AIF1, 1:100, APO8912PU-N, Acris) and cerebral vessels (laminin, 1:300, L9393, Sigma-Aldrich) were visualized and stereologically quantified in 10 sections (with 100 μm interspace between sections) per staining and animal as previously described (27). Briefly, Aβ plaque load was determined at 200× magnification. Aβ plaque volume (ie, percentage of cerebral volume covered by deposits) and Aβ plaque number (n/mm^2) were calculated in an unbiased manner by area fraction fractionator and fractionator (counting frame and grid size each 500 × 500 μm), respectively. The number of microglia with a visible soma and blood vessel bifurcations (n/mm^2) [(vessel ends + vessel branch point)/2] were determined at 200× magnification via fractionator (counting frame 250 × 250 μm, grid size 375 × 375 μm). Additionally, eight sections per animal were co-stained for Aβ plaques and dystrophic neurites (AT8, 1:80, MN1020, Thermo Scientific). The average number of neuritic AT8-positive Aβ plaques was calculated using the fractionator probe (counting frame 250 × 250 μm, grid size 375 × 375 μm) at 200× magnification. Six sections per animal were co-stained for Aβ plaques and microglia. The average number of microglia surrounding one diffuse or core plaque and the number of microglia-negative plaques was calculated using the fractionator probe (counting frame 300 × 300 μm, grid size 425 × 425 μm) at 200× magnification. Absolute values were related to the investigated area (Stereo Investigator 11, MicroBrightField). A Nikon 80i microscope, a color digital camera (3/4" chip, 36-bit color, DV-20, MicroBrightField) and MicroBrightField software were used.

The severity of amyloid angiopathy was determined semi-quantitatively in eight sections per animal at 400× magnification. Leptomeningeal and intracerebral blood vessels with a visible lumen and diameter ≥ 0.01 mm were counted. Blood vessels were classified as amyloid burdened when Aβ-immunoreactivity was present in a circumferential or patchy pattern within the vessel walls. The percentage of Aβ-positive vessels was calculated in relation to total vessel count.

Neuron reconstruction

The effect of sex and genotype on structural neuronal plasticity was tested in Golgi-Cox impregnated coronal sections of aged mice (P372, consecutively designated as P360). 10 pyramidal neurons from layer V frontal cortex (+4 to +1.5 Bregma) were analyzed per animal. All apical and basal dendrites extending from the neuron soma were traced (Neurolucida 11, MicroBrightField) at 400× magnification for 3D reconstruction. To evaluate dendritic spine density, spines were counted on four 20 μm long dendritic segments per neuron, that is, on a proximal apical segment, on a distal apical segment, on a proximal basal segment and on a distal basal segment at 1000× magnification. A proximal segment was defined to start after the first dendritic branch point, a distal one after the third branch point. A morphometric analysis of dendritic number, length and branching complexity was performed. Dendritic complexity was determined by the calculation: (sum of the terminal orders + number of terminals) × (total dendritic length/number of primary dendrites); with terminals defined as dendritic endings and the terminal order defined as the number of "sister" branches encountered while proceeding from the terminal to the cell body (NeuroExplorer, MicroBrightField).

In vitro treatment of differentiated SH-SY5Y neuroblastoma cells or microglial BV-2 cell lines with sex hormones

Human SH-SY5Y cells were neuronally differentiated for 6 days until 7 days *in vitro* (DIV7) by cultivation in DMEM-F12 medium (including glutamine/GlutaMAX, #31331-028, Gibco, Thermo Fisher Scientific) supplemented with 2% fetal bovine serum (FBS, S0115, Merck Millipore) and retinoic acid (RA, 10 μM, R2625, Sigma-Aldrich). At DIV7, cells (100 000 cells per well for lysates, 50 000 cells per well for cell viability monitoring) were cultivated in DMEM-F12 without FBS and RA and treated either with β-estradiol [β-E2, 10 nM, 100 nM, 200 nM, 300 nM, E2758-250MG, Sigma-Aldrich, diluted in EtOH at a final concentration (v/v) of 1%], or with equimolar concentrations of dihydroxy-testosterone (DHT, A8380-1G, Sigma-Aldrich, diluted in EtOH at a final concentration (v/v) of 1%), or with 1% EtOH as control until DIV14.

Murine BV-2 microglia were cultivated until DIV2 in DMEM-F12 medium containing 2% FBS (10^6 cells per well for lysates, 50 000 cells per well for viability testing). Subsequently, microglia were treated with β-E2 or DHT (10 nM, 100 nM, 200 nM, 300 nM) for 48 h, followed by simultaneous incubation with Aβ$_{42}$ peptides (100 nM, AS-72.071, SensoLyte Fluorescent Aβ$_{42}$ Sampler Kit, Anaspec) for an additional 6 or 24 h. Following hormonal treatment, neuronal or microglial cells were either lysed and proteins extracted for KLK8 protein quantification via anti-KLK8 immunoblot (1:200, ABIN759116, antibodies-online.com) or cell viability was monitored via a XTT cell viability kit (9095S, Cell Signaling Technology) following manufacturer's instructions. Intramicroglial and extracellular Aβ$_{42}$ peptide levels were further quantified in protein extracts or supernatant using an Aβ$_{42}$ ELISA Kit (KHB3442, Invitrogen) according to manufacturer's instructions (for the experimental design of *in vitro* investigations see Supporting Information Fig. 1).

Statistics

Data are depicted as means ± SEM. Normal distribution of the data sets was tested by 1-sample Kolmogorov–Smirnov test and Q-Q plots. Homogeneity of variance was calculated with the Levene test. Student's *t* test with Bonferroni correction for multiple testing or Mann-Whitney *U*-Test was applied for the analyses of two groups. Multiple groups' comparison was analyzed by 2-way ANOVA with genotype (TG vs. WT) and sex (female vs. male) as between-subject factors and Bonferroni *post hoc* test. A significance level (α) of $P < 0.05$ was selected. All tests were performed utilizing the SPSS 22 software (IBM).

Study approval

Permission for mice breeding and decapitation (AZ 84-02.04.2014.A488) as well as for behavioral testing (G1338/12; AZ 84-02.04.2012.A412) was granted by the local committee LANUV NRW, Germany. All animal experiments were carried out in accordance with the EU Directive 2010/63/EU and complied with the ARRIVE guidelines.
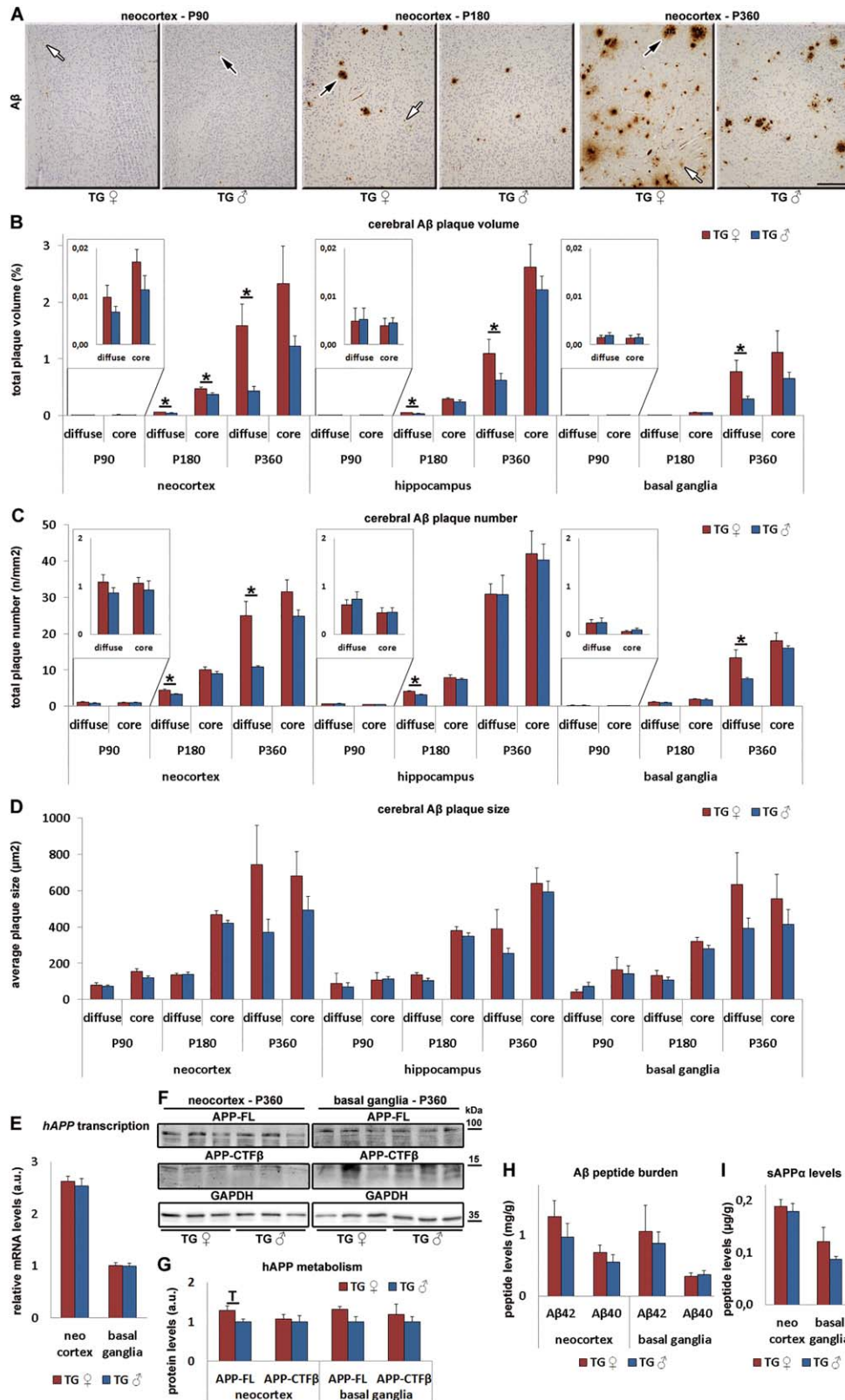
Using post-mortem human material was approved by the ethics committees of the Medical Faculties, University of Duisburg-Essen, (14–5861-BO) and Ludwig-Maximilians-University Munich (#345-13), Germany. Written informed consent was received from the family members of the dead patients before inclusion in the study.

Figure 1. *Female mice show higher levels of Aβ plaque burden compared to males.* **A.** Representative anti-Aβ immunostaining of neocortices illustrating diffuse (white arrows) and core (black arrows) Aβ plaques in transgenic (TG) female (♀) and male (♂) mice around disease onset at the age of 90 days (P90), in a moderate stage of Alzheimer's disease-like pathology at P180 and in a late disease stage at P360. Scale bar: 200 μm. A representative enlarged image of diffuse plaques and core plaques can be found in the Supporting Information Fig. 2A. Stereological quantification of the total diffuse and core plaque volume (**B**), of the total diffuse and core plaque number (**C**) as well as of the average diffuse and core plaque size (**D**) in the neocortex, hippocampus and basal ganglia. **E.** *hAPP* transgene transcription in TG female and male neocortex and basal ganglia at P360. Full-length APP (APP-FL) and C-terminal fragment β (APP-CTFβ) levels (**F**, **G**), Aβ42 and Aβ40 (**H**), and sAPPα peptide levels (**I**) in the neocortex and basal ganglia of female and male TG mice. $^{T}0.05 \leq P < 0.01$, *$P < 0.05$ (Student's *t* test and Bonferroni correction for multiple testing). P90: TG ♀: n = 9, TG ♂: n = 8; P180: TG ♀: n = 8, TG ♂: n = 7; P360: TG ♀: n = 4–7, TG ♂: n = 4–6. Results are shown as mean ± SEM.

RESULTS

Aβ plaque burden becomes more severe in female mice at a moderate disease stage

Pre-existing data about the impact of the sex on the amyloid beta (Aβ) plaque burden in Alzheimer's disease mouse models are controversial. Aβ plaque pathology seems to be increased in female triple transgenic mice (30) at various time points. Conversely, a reduced amount of plaques has been reported around disease onset at P90 in female TgCRND8 mice when compared to males (45).

Here, we quantified the load of core and (their precursors) diffuse Aβ plaques at different disease stages in female and male TgCRND8 mice, in which Aβ plaques (similar to humans) appear first in the neocortex, followed by the hippocampus and then in the basal ganglia. In contrast to (45), we could not show any differences between sexes in the (negligibly low) amount of diffuse and core Aβ plaque load at disease onset (P90) in all three areas (neocortex: diffuse plaque volume: $P = 0.352$; diffuse plaque number: $P = 0.29$; diffuse plaque size: $P = 0.707$; core plaque volume: $P = 0.162$; core plaque number: $P = 0.553$; core plaque size: $P = 0.115$; hippocampus: diffuse plaque volume: $P = 0.93$; diffuse plaque number: $P = 0.559$; diffuse plaque size: $P = 0.767$; core plaque volume: $P = 0.779$; core plaque number: $P = 0.969$; core plaque size: $P = 0.941$; basal ganglia: diffuse plaque volume: $P = 0.602$; diffuse plaque number: $P = 0.939$; diffuse plaque size: $P = 0.318$; core plaque volume: $P = 0.949$; core plaque number: $P = 0.47$; core plaque size: $P = 0.793$) (Figure 1A–D).

A sex-specific difference in plaque load became evident first in a moderate disease stage at P180. At this age, female in comparison to male mice showed an increased volume and number but not size of diffuse and core Aβ plaques in the neocortex (diffuse plaque volume: +33%, $P = 0.028$; diffuse plaque number: +32%, $P = 0.023$; diffuse plaque size: $P = 0.903$; core plaque volume: +27%, $P = 0.023$; core plaque number: $P = 0.277$; core plaque size: $P = 0.116$). In the hippocampus, diffuse plaque load (plaque volume: +49%, $P = 0.027$; plaque number: +28%, $P = 0.017$; plaque size: $P = 0.149$) but not the core plaque burden (plaque volume: $P = 0.157$; plaque number: $P = 0.643$; plaque size: $P = 0.322$) was higher in females than in males. At this stage of the disease the plaque load was still not influenced by sex in the basal ganglia (diffuse plaque volume: $P = 0.257$; diffuse plaque number: $P = 0.194$; diffuse plaque size: $P = 0.494$; core plaque volume: $P = 0.471$; core plaque number: $P = 0.979$; core plaque size: $P = 0.223$) (Figure 1A–D).

Sex differences became much stronger when mice reached an advanced disease at P360. There was a drastic increase in the volume (neocortex: +265%, $P = 0.028$; hippocampus: +75%, $P = 0.038$; basal ganglia: +161%, $P = 0.044$) and partially also the number (neocortex: +129%, $P = 0.013$; hippocampus: $P = 0.501$; basal ganglia: +75%, $P = 0.04$) but not the size (neocortex: $P = 0.179$; hippocampus: $P = 0.221$; basal ganglia: $P = 0.283$) of diffuse Aβ plaques in all three brain areas, whereas the cerebral load of the longer established core plaques did not differ between sexes (neocortex: volume: $P = 0.187$; number: $P = 0.139$; size: $P = 0.304$; hippocampus: volume: $P = 0.23$; number: $P = 0.576$; size: $P = 0.42$; basal ganglia: volume: $P = 0.326$; number: $P = 0.472$; size: $P = 0.436$) (Figure 1A–D).

To test whether the dramatic increase in Aβ plaque load in 1-year-old females was caused by changes in cerebral APP metabolism, we first determined the transcription of the *hAPP* transgene. A sex-specific difference in *hAPP* transcription was neither detectable in the neocortex ($P = 0.676$) nor in the basal ganglia ($P = 0.93$) (Figure 1E). Next, we quantified protein levels of full-length APP (APP-FL), its amyloidogenic and non-amyloidogenic processing products APP C-terminal fragment β (CTFβ), Aβ40 and Aβ42 as well as sAPPα. APP-FL levels were reduced by trend in male neocortices (–23%, $P = 0.078$) while APP-FL levels in basal ganglia ($P = 0.112$) as well as neocortical and basal ganglia CTFβ (neocortex: $P = 0.752$; basal ganglia: $P = 0.61$) (Figure 1F,G), Aβ40 (neocortex: $P = 0.465$; basal ganglia: $P = 0.797$), Aβ42 (neocortex: $P = 0.429$; basal ganglia: $P = 0.698$) (Figure 1H) and sAPPα (neocortex: $P = 0.701$; basal ganglia: $P = 0.271$) peptide levels (Figure 1I) remained unaffected by sex. These results suggest that increased Aβ plaque burden in female brains was neither caused by anabolic (transcription and translation) nor catabolic (processing) differences in *hAPP* metabolism, indicating hampered Aβ clearance and/or intensified Aβ aggregation as a reason for increased Aβ plaque burden in diseased females.

Female mice display higher levels of neurovascular dysfunction already at a moderate disease stage

In a next step, we asked whether increased Aβ plaque load in female transgenic brains might be a cause or consequence of exacerbated neurovascular dysfunction. Therefore, we quantified the blood vessel branching as an indicator of cerebral angiogenesis in female and male transgenic and wildtype mice at the age of P90 (around disease onset), P180 (moderate disease stage) and P360 (late disease stage).

At P90, cerebral vessel density was neither affected by the sex (neocortex: $P = 0.562$; hippocampus: $P = 0.411$; basal ganglia:
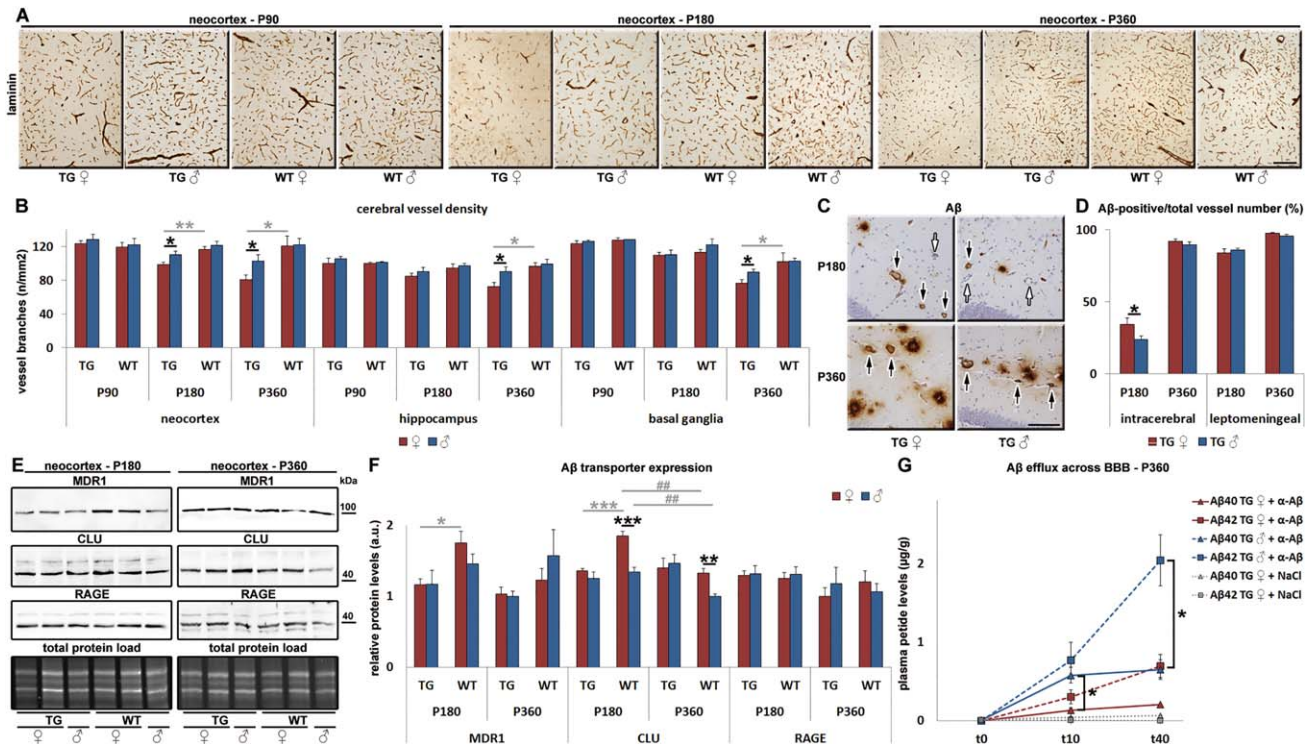
Figure 2. *Increased neurovascular dysfunction in female TgCRND8 mice.* **A.** Anti-laminin immunostaining of neocortices visualizes blood vessels in transgenic (TG) and wildtype (WT) female (♀) and male (♂) mice around disease onset at P90, in a moderate stage of disease at P180 and in a late disease stage at P360. Scale bar: 200 μm. **B.** Stereological quantification of the cerebral vessel branching density in the neocortex, hippocampus and basal ganglia of TG and WT females and males. **C.** Anti-Aβ immunostaining highlighting cerebral amyloid angiopathy in TG brains of both sexes at P180 and P360. **D.** Determination of the ratio (%) of Aβ-positive intracerebral or leptomeningeal vessels in relation to total vessel number at P180 and P360 in TG female and male mice. **E** and **F**. Protein levels of the Aβ efflux transporters MDR1 and CLU as well as of the influx receptor RAGE in neocortices of TG and WT mice of both sexes at P180 and P360. **G.** Aβ efflux dynamics across the blood-brain-barrier (BBB) were quantified over different time spans ($t_0 = 0$ minute = before anti-Aβ antibody (α-Aβ) injection = baseline plasma Aβ levels; $t_{10} = 10$ minutes following α-Aβ injection and t_{40}). *$P < 0.05$, **$P < 0.01$, ***$P < 0.001$ [2-way ANOVA and Bonferroni post hoc test for four-groups comparison as in (B) and (F), Student's *t*-test with Bonferroni correction for two-groups comparison as in (D) and (G)]. Black asterisks indicate comparison between female and male groups, gray asterisks indicate comparison between age- and sex-matched TG and WT mice and gray hash keys indicate comparison between different disease and age stages within sex-matched diseased or control groups. P90: n = 3 per group; P180: TG ♀: n = 7–8, TG ♂: n = 7, WT: n = 7 per sex; P360: TG ♀: n = 4–7, TG ♂: n = 4–6, WT: n = 5 per sex. Results are shown as mean ± SEM.

$P = 0.563$) nor the genotype (neocortex: $P = 0.4$; hippocampus: $P = 0.645$; basal ganglia: $P = 0.375$) (Figure 2A,B).

At P180, a moderate decrease in vessel density became evident first in the neocortex of female in comparison to male transgenics (-11%, $P = 0.035$) and also in comparison to female wildtypes (-15%, $P = 0.004$), whereas neocortical vessel density remained equal between transgenic and wildtype males ($P = 0.128$) and also between female and male wildtypes ($P = 0.42$). There were no differences between the vessel density of sexes (hippocampus: $P = 0.36$; basal ganglia: $P = 0.378$) or genotypes (hippocampus: $P = 0.06$; basal ganglia: $P = 0.189$) in the hippocampus and basal ganglia of 180 days old mice (Figure 2A,B).

At the age of 1 year, vessel density was severely reduced in female compared to male transgenics (neocortex: -22%, $P = 0.04$; hippocampus: -20%, $P = 0.035$; basal ganglia: -15%, $P = 0.039$). Furthermore, vessel density drastically declined in transgenic vs. wildtype females (neocortex: -33%, $P = 0.013$; hippocampus: -25%, $P = 0.012$; basal ganglia: -25%, $P = 0.025$). In contrast,

vessel branching remained stable between transgenic and wildtype males (neocortex: $P = 0.174$; hippocampus: $P = 0.271$; basal ganglia: $P = 0.189$) and was also unaffected by sex in wildtypes (neocortex: $P = 0.174$; hippocampus: $P = 0.271$; basal ganglia: $P = 0.189$) (Figure 2A,B).

The fact that vessel density reduction occurred simultaneously (in the neocortex) or even subsequently (in the hippocampus) to increased Aβ plaque burden indicates that impaired angiogenesis is rather a consequence than a cause of elevated Aβ pathology in transgenic females.

Next, we determined the severity of cerebral amyloid angiopathy (CAA), that is, the proportion (%) of Aβ-positive blood vessels in transgenics at 6 months and 1 year of age. At 6 months, the CAA burden was increased in intracerebral vessels of female vs. male transgenics ($+45\%$, $P = 0.043$), whereas the burden of leptomeningeal CAA did not differ between both sexes ($P = 0.273$). In 1-year-old mice, when a vast proportion of blood vessels were Aβ-positive (range from 89% to 98%), no more sex-specific effects
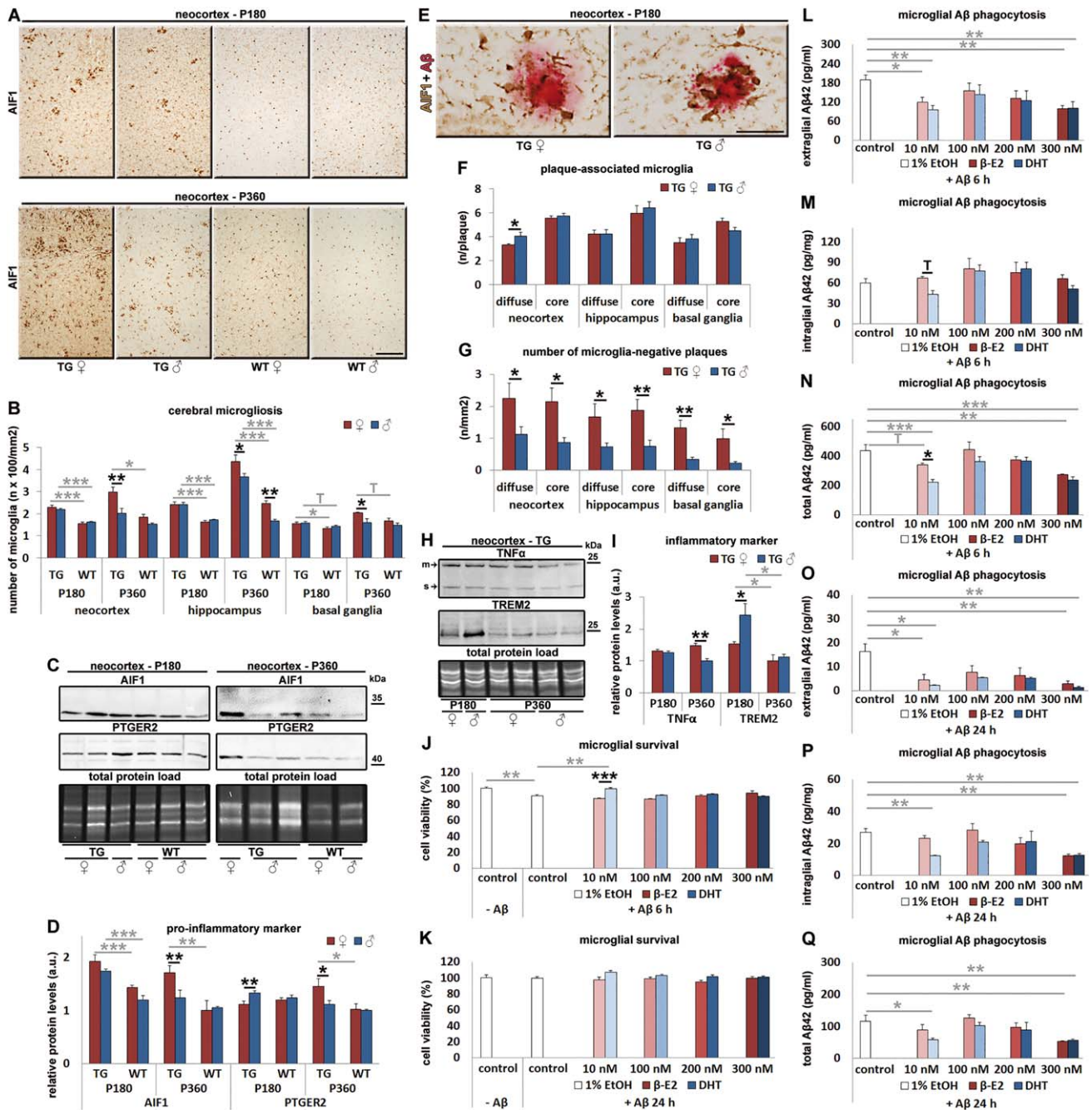
on intracerebral (*P* = 0.339) and leptomeningeal (*P* = 0.137) CAA was detectable (Figure 2C,D).

Additionally, we determined the effect of the sex and the genotype on the neocortical expression pattern of the blood-brain-barrier (BBB) located Aβ efflux transporter MDR1, of the Aβ efflux facilitating clusterin (CLU, also known as apolipoprotein j) and of the influx receptor RAGE in 6 months and 1-year-old mice. Neocortical MDR1 expression was not affected by the sex (*P* = 0.361) but the genotype (*P* = 0.01) when mice reached 6 months; with MDR1 levels being reduced in transgenic vs. healthy females (–34%, *P* = 0.012), whereas at 1 year of age, MDR1 expression did not

differ between any of the four groups tested (*P* = 0.237). CLU expression was modulated by the sex (*P* = 0.00038) and the genotype (*P* = 0.001) in P180 old mice, with CLU levels being elevated in female vs. male wildtypes (+37%, *P* = 0.000094) and reduced in transgenic vs. healthy females (–27%, *P* = 0.000091). At P360, CLU expression was influenced by the sex (*P* = 0.022) but not the genotype (*P* = 0.241), with CLU levels being increased in female in comparison to male wildtypes (+33%, *P* = 0.008). In accordance with a previous publication (67), CLU levels declined during physiological aging (from 6 months to 1 year of age) in wildtype females (–28%, *P* = 0.008) and males (–26%, *P* = 0.002). RAGE quantities

Figure 3. *Female mice display higher levels of neuroinflammation and female sex hormone is less effective in promoting microglial degradation activity.* **A.** Anti-AIF1 immunostaining showing microglia in the neocortex of transgenic (TG) and wildtype (WT) females (♀) and males (♂) at the age of P180 or P360. Scale bar: 200 μm. **B.** Stereological quantification of the number of AIF1-positive microglia in the neocortex, hippocampus and basal ganglia of adult and aged, diseased and healthy female and male mice. **C** and **D.** Protein expression of the inflammatory markers AIF1 and PTGER2 in neocortices of TG and WT mice of both sexes at P180 and P360. **E.** Neocortical double immunostaining against AIF1 (brown) and Aβ (red) in P180 old female and male TG mice. Scale bar: 50 μm. The average number of microglia that surround a single diffuse or core Aβ plaque (**F**) and the number of microglia-negative diffuse or core Aβ plaques (**G**) located in the neocortex, hippocampus or basal ganglia of P180 old TG female and male mice. A representative image of a diffuse plaque and core plaques surrounded by microglia can be found in the Supporting Information Fig. 2B. **H** and **I.** Protein expression of the inflammatory markers TNFα and TREM2 in TG neocortices of both sexes at P180 and P360.

A combined quantification of the membrane-bound form of TNFα (m) and soluble TNFα (s) is depicted. **J** and **K.** Cell viability monitoring (XTT assay) of ethanol (EtOH, control), β-estradiol (β-E2) or dihydroxytestosterone (DHT)-treated BV-2 microglia incubated with $A\beta_{42}$ for 6 h (J) or 24 h (K). **L–Q.** Quantification of extracellular (L, O), intramicroglial (M, P), or total (N, Q) $A\beta_{42}$ levels from BV-2 microglia cultures either treated with EtOH, β-E2 or DHT and incubated with $A\beta_{42}$ for 6 h (L–N) or 24 h (O–Q). $^{T}0.05 \leq P < 0.01$, $*P < 0.05$, $**P < 0.01$, $***P < 0.001$ [2-way ANOVA and Bonferroni post hoc test for multiple-groups comparison as in (B), (D) and (J–Q), Student's *t*-test with Bonferroni correction for two-groups comparison as in (F), (H) and (I)]. Black asterisks indicate comparison between female and male groups or between microglia cultured in β-E2 and microglia treated with DHT, gray asterisks indicate comparison between age- and/or sex-matched TG and WT mice or between cells cultured in control media and cells treated with sexual hormones. P180: n = 7 per group; P360: TG ♀: n = 4–7, TG ♂: n = 5–6, WT: n = 5 per sex. For *in vitro* experiments, six cell culture plates from three independent batches per treatment condition were analyzed. Results are shown as mean ± SEM.

did not differ between all four groups, neither in 6 months ($P = 0.97$) nor in 1-year-old mice ($P = 0.493$) (Figure 2E,F).

Lastly, we investigated the kinetics of Aβ efflux from the brain to blood in 1-year-old transgenics, using an altered protocol from (10). Ten and forty minutes ($= t_{10}$ and t_{40}) following intravenous injection of an Aβ stabilizing anti-Aβ antibody, blood plasma Aβ levels were measured. In female plasma, the accumulation of $A\beta_{40}$ (-77%, $P = 0.03$) and $A\beta_{42}$ (-66%, $P = 0.04$) was drastically reduced after 10 (t_{10}), and 40 minutes (t_{40}), respectively, when compared to male's blood, indicating faulty Aβ peptide clearance across the BBB in transgenic females (Figure 2G).

In summary, these findings suggest that reduced vessel density and concomitant impairment in Aβ clearance might be a female-specific complication in Alzheimer's disease which is caused by and contributes to elevated Aβ plaque burden.

Neuroinflammation is more pronounced in transgenic females at a late disease stage

We also tested whether the cerebral inflammation status differed between female and male mice. Therefore, we first counted the number of allograft inflammatory factor 1 (AIF1) expressing microglia in the neocortex, hippocampus and basal ganglia.

Until 6 months of age, a sex-specific difference in microgliosis could not be detected (in transgenics neocortex: $P = 0.296$; hippocampus: $P = 0.968$; basal ganglia: $P = 0.728$; in wildtypes neocortex: $P = 0.602$; hippocampus: $P = 0.559$; basal ganglia: $P = 0.293$), whereas a disease-related microgliosis induction was evident irrespective of the sex in the neocortex (females: $+47\%$, $P = 0.0000003$; males: $+35\%$, $P = 0.00001$) and hippocampus (females: $+48\%$, $P = 0.000024$; males: $+41\%$, $P = 0.000097$) and to a lesser extend also in the basal ganglia (significantly in females: $+17\%$, $P = 0.018$; but only by trend in males: $+11\%$, $P = 0.09$) (Figure 3A,B).

First at the age of 1 year an increased microgliosis was detectable in female vs. male transgenic neocortex ($+59\%$, $P = 0.006$), hippocampus ($+19\%$, $P = 0.02$) and basal ganglia ($+27\%$, $P = 0.044$). Sex-specific differences in wildtypes could be detected

only in the hippocampus of 1-year-old mice with females exhibiting an increased microgliosis when compared to males (hippocampus: $+47\%$, $P = 0.006$; neocortex: $P = 0.405$; basal ganglia: $P = 0.311$). A significant disease-related microgliosis was detectable in the neocortex ($+53\%$, $P = 0.01$) and in the hippocampus ($+77\%$, $P = 0.000003$) but not significantly in basal ganglia ($+21\%$, $P = 0.096$) of female mice while in males this pathology was restricted to the hippocampus ($+118\%$, $P = 0.0000008$; neocortex: $P = 0.549$; basal ganglia: $P = 0.562$) (Figure 3A,B).

Additionally, we determined the neocortical protein expression of AIF1 and of the pro-inflammatory prostaglandin E receptor 2 (PTGER2). In line with morphometry results, AIF1 protein levels did not differ significantly between females and males irrespective of genotype until P180 (transgenics: $P = 0.125$; wildtypes: $P = 0.079$), while genotype differences (transgenic vs. wildtype) were evident in both sexes (females: $+35\%$, $P = 0.00031$; males: $+45\%$, $P = 0.0002$). Sex differences became apparent at P360 only in transgenics (female vs. male: $+37\%$, $P = 0.008$) but not in healthy animals ($P = 0.88$) (Figure 3C,D). Neocortical PTGER2 levels were elevated in the 6-month-old male vs. female transgenics ($+20\%$, $P = 0.007$) but not in wildtypes ($P = 0.582$) and remained unaffected by the genotype in females ($P = 0.267$) and males ($P = 0.254$). When mice reached 1 year of age, elevated concentrations of PTGER2 were detectable in disease-affected females vs. males ($+31\%$, $P = 0.042$), whereas PTGER2 levels were not affected by sex in wildtype controls ($P = 0.886$). Furthermore, PTGER2 levels were increased in diseased in comparison to healthy females ($+42\%$, $P = 0.018$) but remained unchanged between transgenic and wildtype males ($P = 0.514$) (Figure 3C,D).

Taken together, the female-specific induction of cerebral inflammation is rather a consequence of elevated Aβ plaque burden than its cause since it occurs later (at P360) than the emergence of sex-specific differences in Aβ pathology (at P180). Independent from the causality order, inflammation can perpetuate Aβ aggregation and therefore exacerbate Aβ plaque pathology in late disease stages.

Microglial Aβ plaque penetration is less pronounced in females

Based on the fact that at 6 months of age the total number of microglia did not differ between female and male transgenics (Figure 3A,B) although the Aβ plaque load was already increased in diseased females (Figure 1A–C), we were prompted to test whether microglial distribution was different between the sexes. We therefore quantified the density of microglia surrounding/infiltrating Aβ plaques in both sexes at P180. Double-immunostaining against AIF1 and Aβ and subsequent stereological quantification revealed that the number of microglia infiltrating core plaques was higher than those surrounding diffuse plaques. Furthermore, neocortical diffuse (but not core) plaques of males were surrounded by a larger number of microglia when compared to females ($+19\%$, $P = 0.039$) (Figure 3E,F). Strikingly, females showed in general more diffuse and core plaques which were completely void of microglia when compared to males (neocortex: diffuse plaques: $+100\%$, $P = 0.037$; core plaques: $+148\%$, $P = 0.011$; hippocampus: diffuse plaques: $+130\%$, $P = 0.028$; core plaques: $+153\%$, $P = 0.008$; basal ganglia: diffuse plaques: $+298\%$, $P = 0.001$; core plaques: $+361\%$, $P = 0.017$) (Figure 3E,G). To further analyze whether the microglial phenotype (ie, pro-inflammatory, cytotoxic vs. phagocytic/neuro-protective) was influenced by the sex, we determined the expression of the tumor necrosis factor alpha (TNFα), which is induced in pro-inflammatory microglia (66) and astrocytes (26), and of the triggering receptor expressed on myeloid cells 2 (TREM2), which is up-regulated in neuro-protective microglia (15) and promotes microglial metabolic/phagocytic function in Alzheimer's disease (62), in the cortex of female and male transgenics at P180 and P360. TNFα levels were higher in females ($+48\%$, $P = 0.003$) at P360 (but not earlier) when compared to males, whereas, TREM2 levels were down-regulated in female transgenics already at P180 (-37%, $P = 0.041$). At P360 (with disease progression), TREM2 levels dropped further in both sexes (females: -35%, $P = 0.035$; males: -54%, $P = 0.014$), resulting in similar TREM2 amounts between female and male mice ($P = 0.619$) (Figure 3H,I).

To summarize, microglial attraction toward Aβ plaques and/or microglial survival in the presence of Aβ plaques seem to be more severely impaired in female mice. Increased TNFα and decreased TREM2 levels further hints at higher cytotoxic and lower phagocytic activity of microglia which would explain a reduced microglial Aβ degradation efficacy in female brain.

β-Estradiol in contrast to testosterone has a reduced potential to protect microglia from Aβ toxicity and to promote Aβ degradation

As the number of microglia surrounding Aβ plaques and TREM2 levels were reduced in transgenic females, we next quantified the survival rate and the Aβ phagocytosis efficacy in the microglia cell line BV-2 that was first either pre-treated with the female-prevalent sex hormone β-estradiol (β-E2) or the male-prevalent sex hormone dihydroxy-testosterone (DHT, which, in contrast to testosterone, does not undergo aromatisation to estrogen) for 48 h, followed by co-incubation with Aβ$_{42}$ peptides for another 6 or 24 h (for experimental design see Supporting Information Fig. 1A).

When microglia, only treated with hormone diluent EtOH, were incubated with 100 nM Aβ$_{42}$ for 6 h, a moderate but significant drop in cell survival could be detected when compared to control culture solely treated with EtOH but not with Aβ$_{42}$ (-9%, $P = 0.002$). Interestingly, a low concentration of DHT (10 nM) in comparison to control treatment with EtOH could protect microglia from Aβ$_{42}$ induced cell death as it increased cell survival ($+10\%$, $P = 0.004$) reaching viability levels observed in microglia not exposed to Aβ$_{42}$ (10 nM DHT plus Aβ$_{42}$ incubation vs. EtOH treatment without Aβ$_{42}$ incubation: $P = 0.809$). Neither higher DHT levels (100 nM DHT vs. EtOH plus Aβ$_{42}$ incubation: $P = 0.748$; 200 nM DHT vs. EtOH plus Aβ$_{42}$ incubation: $P = 0.423$; 300 nM DHT vs. EtOH plus Aβ$_{42}$ incubation: $P = 0.851$) nor any tested β-E2 concentration (10 nM β-E2 vs. EtOH plus Aβ$_{42}$ incubation: $P = 0.234$; 100 nM β-E2 vs. EtOH plus Aβ$_{42}$ incubation: $P = 0.114$; 200 nM β-E2 vs. EtOH plus Aβ$_{42}$ incubation: $P = 0.931$; 300 nM β-E2 vs. EtOH plus Aβ$_{42}$ incubation: $P = 0.3$) could exert cellular protection. Accordingly, microglial viability was strengthened following treatment with a low concentration (10 nM) of DHT when compare to treatment with equimolar β-E2 ($+14\%$, $P = 0.0001$) (Figure 3J). Twenty-four hours following Aβ$_{42}$ incubation, microglial viability completely recovered from Aβ$_{42}$ induced toxicity, as no differences in cell survival rates could be detected in any of the treatment groups ($P = 0.325$) (Figure 3K).

Furthermore, we determined the impact of sex hormones on microglial Aβ phagocytosis and clearance efficacy. Therefore, we separately quantified intramicroglial (phagocytosed) and extramicroglial Aβ$_{42}$ peptide levels 6 and 24 h following addition of Aβ$_{42}$ in microglial culture either treated with β-E2 or DHT.

Six hours after Aβ peptides had been added to the medium, the concentration of extraglial Aβ peptides still remaining in the supernatant (and not been phagocytosed yet) was decreased following treatment with low or high amounts of β-E2 or DHT in comparison to EtOH incubation (10 nM β-E2 vs. EtOH: -38%, $P = 0.034$; 10 nM DHT vs. EtOH: -50%, $P = 0.006$; 300 nM β-E2 vs. EtOH: -48%, $P = 0.008$; 300 nM DHT vs. EtOH: -47%, $P = 0.009$) but did not differ between β-E2 and DHT administration in any concentration tested ($P = 0.572$) (Figure 3L). Simultaneously, intraglial Aβ levels showed only a tendency for reduction following treatment with low concentrations (10 nM) of DHT when compared to incubation with equimolar β-E2 (-36%, $P = 0.065$) (Figure 3M) whereas total (intraglial plus extraglial) levels of Aβ$_{42}$ peptides that had not been degraded after 6 h were strongly reduced in microglial culture treated with low amounts (10 nM) of DHT when compared to EtOH only treatment (-49%, $P = 0.0001$). In contrast, incubation with equimolar β-E2 reduced total Aβ content (indicating net Aβ degradation) only by trend (-22%, $P = 0.059$). Correspondingly, a low concentration of DHT (10 nM) in comparison to equimolar β-E2 improved Aβ degradation and thereby reduced total levels of Aβ (-34%, $P = 0.036$). A boosted microglial Aβ degradation in terms of drop of total Aβ could be also detected following treatment with high concentrations (300 nM) of β-E2 or DHT in comparison to control (EtOH only) culture (β-E2 vs. EtOH: -37%, $P = 0.002$; DHT vs. EtOH: -46%, $P = 0.0003$) (Figure 3N).

Eighteen-hours later (ie, 24 h following addition of Aβ to the supernatant), irrespective of the treatment, more than 75% of all Aβ peptides had been already engulfed and degraded (probably

explaining identical viability rates between microglia not incubated with Aβ and microglia interacting with Aβ for 24 h, see Figure 3K). Nonetheless, at this stage of treatment, an improved degradation (indicated by reduction of total Aβ) could be still detected following treatment with low amounts of DHT (10 nM DHT vs. EtOH: -50%, $P = 0.013$) but not following incubation with equimolar β-E2 (10 nM β-E2 vs. EtOH: $P = 0.225$) (Figure 3Q). Treatment with high concentrations (300 nM) of both sex hormones enhanced Aβ degradation and reduced total Aβ levels (β-E2 vs. EtOH: -55%, $P = 0.006$; DHT vs. EtOH: -52%, $P = 0.009$) (Figure 3O–Q).

To summarize, these results suggest that although at higher concentrations both sexual hormones are capable of facilitating microglial Aβ clearance, at lower concentrations only testosterone (but not estrogen) enables microglia to better resist Aβ toxicity and to improve Aβ clearance. These findings offer an explanation for the increased microglia density around Aβ plaques and the reduced Aβ pathology in transgenic males compared to females.

Cerebral KLK8 levels are increased in murine and human females

Kallikrein-8 (KLK8), a serine protease that participates in neuroplasticity and anxiety generation, is excessively expressed in the brains of Alzheimer's disease patients and TgCRND8 mice even before the onset of the disease and its short-term inhibition attenuates multiple features of Alzheimer's disease pathology in female mice (28). Here, we tested whether KLK8 overexpression might be a female-specific contributor to Alzheimer's disease progression and therefore quantified neocortical protein levels of KLK8 in female and male transgenics and wildtypes between P3 (early postnatal period) and P360 (late disease stage). Until P30 KLK8 expression was not influenced by sex ($P \geq 0.1$). Around 3 months of age, a sex-related effect on the KLK8 expression could be detected as neocortical KLK8 levels were significantly increased in female vs. male transgenics ($+25\%$, $P = 0.025$) but only by trend in wildtypes ($+15\%$, $P = 0.062$). After P180, female and male transgenic mice showed similar levels of KLK8 while in wildtypes female vs. male differences remained still detectable (P180: $+16\%$, $P = 0.038$; P360: $+22\%$, $P = 0.031$) (Figure 4A,B).

In conformity to our previous results (28), a transgene-specific KLK8 overexpression could be detected first at P30 ($+69\%$, $P = 0.001$) in both female ($+71\%$, $P = 0.011$) and male mice ($+66\%$, $P = 0.012$) when compared to sex-matched healthy controls. The KLK8 excess in TgCRND8 vs. wildtype mice lasted (at least) until P360 (P90: $+20\%$, $P = 0.017$; P180: $+12\%$, $P = 0.037$; P360: $+15\%$, $P = 0.014$) (Figure 4C). As previously shown, we could again detect an age-related KLK8 drop in both mouse sexes and genotypes between P3 and P360, possibly as a consequence of reduced neuroplasticity processes in the aging brain. Consistent with higher levels of KLK8 expression, the processing of its substrate fibronectin (56) (indicated by the ratio of fragmented to full-length fibronectin) was elevated in female vs. male wildtypes ($+43\%$, $P = 0.001$) and in transgenic vs. healthy males ($+53\%$, $P = 0.029$) but showed only a trend toward elevation in transgenic vs. healthy females ($+29\%$, $P = 0.074$) at 6 months of age (Figure 4D,E).

In a next step, we evaluated the impact of sex and disease progression on cerebral KLK8 levels in humans [in independent patient cohorts different from those investigated in (28)]. We quantified hippocampal KLK8 protein levels in female and male patients classified as CERAD A/Braak I-II, CERAD B/Braak III-IV, CERAD C/Braak V-VI and in neurologically healthy, age-matched controls utilizing two independent techniques (ELISA and immunoblotting). Both quantification methods revealed that similar to mice, KLK8 levels were drastically increased in women when compared to men, not only in moderate to late Alzheimer's disease stages (ELISA: CERAD C, $+44\%$, $P = 0.047$; immunoblotting: CERAD B, $+113\%$, $P = 0.03$) but also in healthy controls (ELISA: $+71\%$, $P = 0.008$; immunoblotting: $+118\%$, $P = 0.005$) (Figure 4F,H,I). In line with our previous results (28) irrespective of the sex, there was an increasing KLK8 excess during disease progression when compared to controls (ELISA: CERAD A vs. control: $+52\%$, $P = 0.024$, CERAD B vs. control: $+81\%$, $P = 0.036$, CERAD C vs. control: $+62\%$, $P = 0.006$; immunoblotting: by trend in CERAD A vs. control: $+45\%$, $P = 0.076$ and significantly in CERAD B vs. control: $+74\%$, $P = 0.036$ and in CERAD C vs. control: $+95\%$, $P = 0.014$) (Figure 4G,J). Our finding on increased KLK8 levels in females of both species even in the absence of Alzheimer's disease suggests that sex-related hormones might affect KLK8 levels, which in turn could influence the risk for Alzheimer's disease.

Neuronal and microglial KLK8 expression is induced by estradiol but not by testosterone

Next we sought to verify the role of sex hormones on KLK8 expression. Therefore, neuronal and microglial cell lines were either treated with different concentrations of β-E2 or DHT, followed by determination of KLK8 protein levels and cell survival (for experimental setup see Supporting Information Fig. 1B, C). In differentiated SH-SY5Y neuroblastoma cells, β-E2 (vs. EtOH) significantly induced the expression of KLK8 at a concentration of 100 nM ($+41\%$, $P = 0.0003$) or 300 nM ($+28\%$, $P = 0.013$) but not 10 nM ($P = 0.297$) or 200 nM ($+19\%$, $P = 0.09$). In contrast, DHT (vs. EtOH) did not influence neuronal KLK8 levels at any concentration tested (10 nM: $P = 0.509$; 100 nM: $P = 0.825$; 200 nM: $P = 0.863$; 300 nM: $P = 0.906$). Accordingly, KLK8 expression was increased following treatment with 100 nM β-E2 when compared to equimolar incubation with DHT ($+44\%$, $P = 0.00041$) (Figure 4K,L). Also the microglial cell line BV-2 reacted with KLK8 up-regulation following β-E2 treatment. Similar to neurons, β-E2 but not DHT was able to increase KLK8 levels also in microglial cells, whereby here 10 nM ($+26\%$, $P = 0.015$) and 100 nM ($+22\%$, $P = 0.036$) but not 200 nM ($P = 0.934$) or 300 nM ($P = 0.669$) concentrations were effective. Accordingly, microglial KLK8 expression tended to be increased following treatment with 10 nM or 100 nM β-E2 when compared to equimolar incubation with DHT (10 nM: $+19\%$, $P = 0.059$; 100 nM: $+19\%$, $P = 0.066$) (Figure 4M,N). Of note, neither neuronal ($P = 0.182$) nor microglial ($P = 0.268$) survival differed between any of the treatment groups (data not shown).

Spatial memory is impaired more severely in female than male mice

We further determined whether the above-named sex-specific differences in Alzheimer's disease-related pathology, might also affect
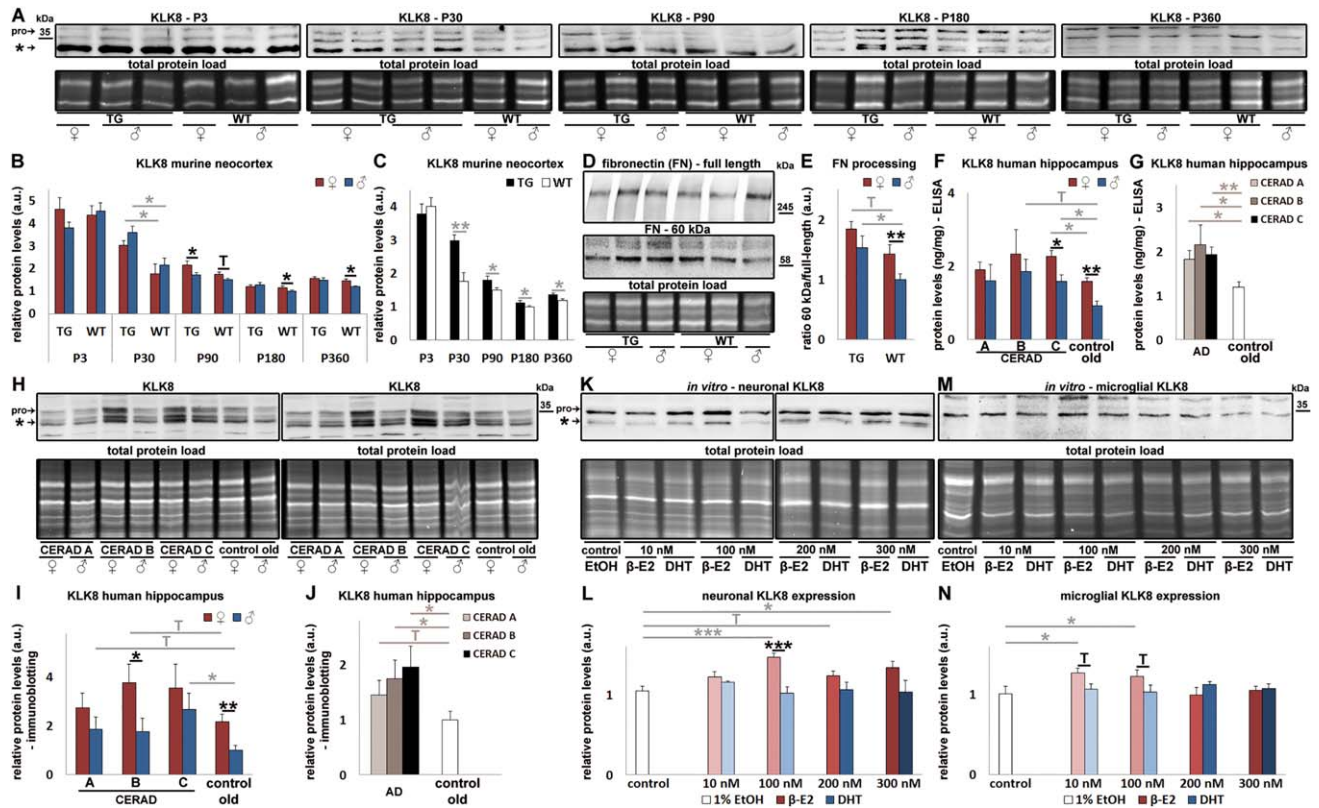
Figure 4. *KLK8 levels are higher in female brain and female sex hormone increases KLK8 in neuronal/glial cells.* **A–C.** Neocortical KLK8 protein levels of transgenic (TG) and wildtype (WT) females (♀) and males (♂) between P3 and P360. **D** and **E.** Neocortical processing of the KLK8 substrate fibronectin in P180 old TG and WT female and male mice, calculated by the ratio of a 60 kDa fibronectin processing product and full-length fibronectin. **F–J.** Hippocampal KLK8 levels of female and male Alzheimer's disease patients at CERAD A/Braak I–II, CERAD B/Braak III–IV, CERAD C/Braak V–VI stages and age-matched controls quantified by ELISA (F, G) or immunoblotting (H–J). KLK8 expression in differentiated SH-SY5Y neuroblastoma cells (**K**, **L**) or in microglial BV-2 cells (**M**, **N**) following treatment with ethanol (EtOH, control), β-estradiol (β-E2) or dihydroxytestosterone (DHT). A combined quantification of the pro-form of KLK8 and activated KLK8* is depicted for murine and human samples and for protein lysates from cell cultures. $^{T}0.05 \leq P < 0.01$, $*P < 0.05$,

$**P < 0.01$, $***P < 0.001$ [2-way ANOVA and Bonferroni post hoc test for multiple-groups comparison as in (B), (E), (F), (G), (I), (J), (L) and (N), Student's *t*-test with Bonferroni correction for two-groups comparison as in (C)]. Black asterisks indicate comparison between female and male groups or between cells cultured with β-E2 and cells treated with DHT, gray asterisks indicate comparison between age- and sex-matched TG and WT mice or between diseased and healthy patients or between cells cultured in control media and cells treated with sexual hormones. P3: n = 6 per group; P30: TG ♀: n = 8, TG ♂: n = 6, WT: n = 4 per sex; P90: n = 9 per group; P180: TG ♀: n = 8, TG ♂: n = 7, WT: n = 7 per sex; P360: TG ♀: n = 7, TG ♂: n = 6, WT ♀: n = 6, WT ♂: n = 5; CERAD A: ♀: n = 7, ♂: n = 6; CERAD B: ♀: n = 6, ♂: n = 7; CERAD C: ♀: n = 5, ♂: n = 6; control old: ♀: n = 10, ♂: n = 13. For *in vitro* experiments, 6 to 10 cell culture plates from five independent batches per treatment condition were analyzed. Results are shown as mean ± SEM.

cognitive impairments in a sex-specific manner. Accordingly, transgenics (along with their age-matched healthy littermates) were phenotyped for avoidance and exploratory behavior in the Open Field test and for spatial learning and memory in the Barnes Maze in an advanced disease stage (P360).

Automated video tracking analysis confirmed a previously shown (3, 4, 29) disease-related agitation in both female and male TgCRND8 mice at 1 year of age, indicated by circling hyperactive movements, an increased distance travelled and an elevated number of visits in the Open Field arena. In contrast, sex-related differences in avoidance and exploratory behavior were not detectable at this age, neither in transgenics nor in wildtypes (Figure 5A–C).

Analysis of the Barnes Maze revealed that at 1 year of age, spatial learning and memory performance was impaired between

the first and the fourth testing day in female vs. male mice irrespective of their genotype, indicated by increased total latencies (Figure 5D–F), errors made (Figure 5D,G,H) or distances covered (Figure 5D,I,J). Simultaneously, we could confirm a disease-related performance deficit in transgenic mice of both sexes (Figure 5D–J). Sex and genotype differences in spatial memory performance were not accompanied by changes in motor skills, as the average velocity (in cm/s) between the four groups did not differ significantly at any test day (day 1: transgenic females: 7.84 ± 1.38, transgenic males: 5.94 ± 0.69, wildtype females: 5.61 ± 0.75, wildtype males: 5.31 ± 0.65, $P = 0.267$; day 2: transgenic females: 6.62 ± 1.09, transgenic males: 8.54 ± 1.78, wildtype females: 7.04 ± 1.12, wildtype males: 5.27 ± 1.12, $P = 0.463$; day 3: transgenic females: 7.85 ± 2.48, transgenic
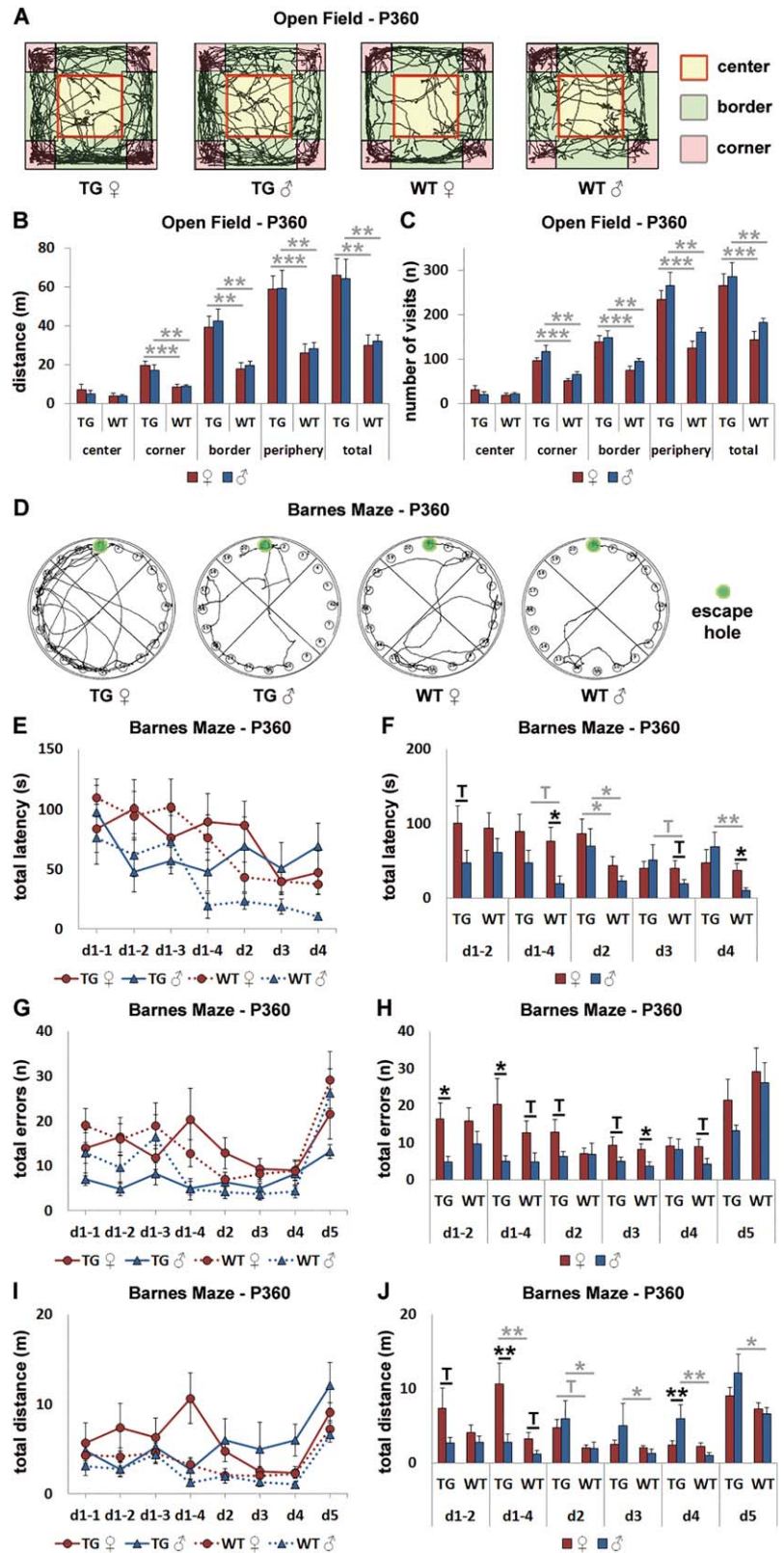
Figure 5. *Spatial memory is impaired more severely in female than male mice.* Representative paths in the Open Field (**A**) and the Barnes Maze (**D**, test day 1, trial 4 [d1–4] from transgenic (TG) and wildtype (WT) females (♀) and males (♂) at the age of P360. **B.** Distance mice travelled in the center area, borders and corners of the Open Field platform as well as the total distance mice covered during the Open Field test. **C.** Number of visits in all three compartments of the Open Field platform and summarized visits. Learning curves during spatial training in the Branes Maze (**E**, **G**, **I**). Total time (E, **F**), number of wrong holes approximated (G, **H**) and total distance (I, **J**) mice needed to escape from the Barnes Maze arena between d1-t2 and d5. $^T 0.05 \leq P < 0.01$, $^* P < 0.05$, $^{**} P < 0.01$, $^{***} P < 0.001$ (2-way ANOVA and Bonferroni post hoc test). Black asterisks indicate comparison between female and male groups, gray asterisks indicate comparison between age- and sex-matched TG and WT mice. TG ♀: n = 9, TG ♂: n = 6, WT ♀: n = 12, WT ♂: n = 10. Results are shown as mean ± SEM.

males: 8.33 ± 1.43, wildtype females: 7.14 ± 1.24, wildtype males: 5.06 ± 0.68, $P = 0.511$; day 4: transgenic females: 7.11 ± 1.97, transgenic males: 7.44 ± 1.33, wildtype females: 6.77 ± 1.22, wildtype males: 6.55 ± 1, $P = 0.982$; day 5: transgenic females: 10.04 ± 1.28, transgenic males: 13.45 ± 2.84, wildtype females: 8.05 ± 0.96, wildtype males: 7.3 ± 0.93, $P = 0.051$).

Structural neuroplasticity is slightly affected in aged female brains

In a next step, we investigated possible sex-specific differences in dendritic branching complexity and spine density in Golgi-Cox-impregnated pyramidal neurons from layer V frontal cortex of 1-year-old female and male transgenic and wildtype mice (utilizing Neurolucida and Neuro Explorer software). Apical dendritic branching complexity was reduced in female vs. male wildtypes (–35%, $P = 0.025$) but only by trend in transgenics (–41%, $P = 0.06$) (Figure 6A,B). Aside from this difference, we could not detect any significant differences between the four groups regarding the basal dendritic complexity ($P = 0.574$) (Figure 6A,B), dendritic arborization (number of basal dendrites: $P = 0.764$; number of apical dendrite branches: $P = 0.406$; number of basal dendrite branches: $P = 0.517$) (Figure 6A,C), dendritic outgrowth (apical dendrite length: $P = 0.174$; basal dendrite length: $P = 0.788$) (Figure 6A,D) or spine density (average number of spines per μm dendrite: $P = 0.16$) (Figure 6A,E).

Additionally, we evaluated the influence of the sex on the hippocampal protein expression of structural neuroplasticity marker in 1-year-old diseased and healthy mice. Impaired spatial learning and memory performances in female transgenics (and to a lesser extend wildtypes) were also reflected by reduced hippocampal protein synthesis of the immediate-early gene ARC in comparison to male transgenics (–45%, $P = 0.047$) and female wildtypes (–48%, $P = 0.027$) (Figure 6F,I). In contrast, neither synaptophysin nor GAP43 levels were affected by the sex in diseased (SYP: $P = 0.167$; GAP43: $P = 0.351$) or healthy (SYP: $P = 0.1$; GAP43: $P = 0.12$) mice (Figure 6G–I).

Sex-specific differences do not pertain to all aspects of Alzheimer's disease

Female and male brains are equally burdened with tau pathology

To evaluate the sex-effect on tau pathology, we determined the number of neuritic plaques hallmarked by AT8-positive, dystrophic neurites surrounding Aβ-positive plaques via stereology and neocortical phospho-tau levels via AT8 immunoblotting in 1-year-old transgenics. The number of neuritic plaques in the neocortex ($P = 0.48$) and in the basal ganglia ($P = 0.794$) (Figure 7A,B) as well as the neocortical phospho-tau levels ($P = 0.182$) (Figure 7C,D) remained similar in female and male transgenics, confirming a previous study that demonstrated comparable tau pathology burden between female and male 3xTg-AD mice at various time points (30).

Autophagy is not differentially affected in female and male TgCRND8 brains

Autophagy-mediated intracellular clearance of metabolic debris is impaired in the brains of Alzheimer's disease patients (22) and transgenic mice (64). Accordingly, we tested whether increased Aβ burden in female transgenic brains might be accompanied by propagated autophagy defects. We therefore determined the neocortical levels of beclin-1 [participating in the initiation of autophagosome complexes (21)], ATG5 [essential for the autophagosome assembly (50)] and STX17 [triggers fusion of autophagosomes with lysosomes (32)] in 1-year-old transgenics and wildtypes. Also

with regard to the cerebral expression of autophagy markers, sex-specific differences could not be detected, neither between diseased (beclin-1: $P = 0.473$; ATG5: $P = 0.232$; STX17: $P = 0.256$) nor healthy (beclin-1: $P = 0.482$; ATG5: $P = 0.357$; STX17: $P = 0.908$) female and male mice, whereas a disease-related drop in autophagy marker levels could be determined for beclin-1 (by trend, transgenic vs. wildtype females: -32%, $P = 0.09$) and STX17 (transgenic vs. wildtype males: -27%, $P = 0.014$) (Figure 7E–H).

DISCUSSION

Women have a higher vulnerability for Alzheimer's disease, but the reasons for this sex imbalance are not well understood.

In the present study, we first investigated the influence of sex on multiple aspects of Alzheimer's pathology during the course of disease in the TgCRND8 mouse model. We could show that female in comparison to male transgenics began to display an increased Aβ plaque burden about 3 months after the onset of plaque pathology (P180), simultaneous to the development of an increased neurovascular dysfunction and a reduced microglial density in the vicinity of Aβ plaques, which was followed by aggravated neuroinflammation (P360), diminished structural neuroplasticity and worse spatial memory performance in an advanced disease stage (P360). In contrast to all the above-named sex differences which appeared long after the onset of Aβ plaque pathology, we here for the first time show that cerebral KLK8 levels were already increased in female vs. male transgenics at the very beginning stage of plaque formation (around P90). In a second step, we compared the expression level of KLK8 in female and male AD patients. In line with murine data, higher KLK8 levels could be detected also in brains of female Alzheimer's disease patients in early disease stages (CERAD B, Braak III-IV) compared with their male counterparts. Previous work in our lab has identified KLK8 as a potential key player in the pathogenesis of Alzheimer's disease. There we could demonstrate a very early and multifocal overexpression of KLK8 in disease-affected and less-affected brain areas of transgenic mice and AD patients prior to disease onset. Furthermore, we could show that inhibition of excessive KLK8 attenuates various aspects of the disease such as Aβ and tau pathology, neurovascular dysfunction or autophagy and neuroplasticity impairments, thereby promoting spatial memory performance and diminishing anxiety-like behavior in transgenic mice (28). The female-dominant KLK8 excess at an incipient pathology stage before onset of any other sex-associated differences suggests KLK8 as a potential cause for the increased vulnerability for Alzheimer's disease in particular in females.

Furthermore, we also provide an explanation for higher KLK8 levels in female brains as we could show that β-estradiol but not dihydroxy-testosterone is capable to induce KLK8 production in neuronal and microglial cell lines, suggesting that higher concentrations of β-estradiol from puberty until menopause might be responsible for the long term cerebral KLK8 elevation which in turn could reverse the neuroprotective effects of β-estradiol. Effects of sexual hormones on KLK8 expression have been hitherto described only under neoplastic (36) but not neurodegenerative conditions.
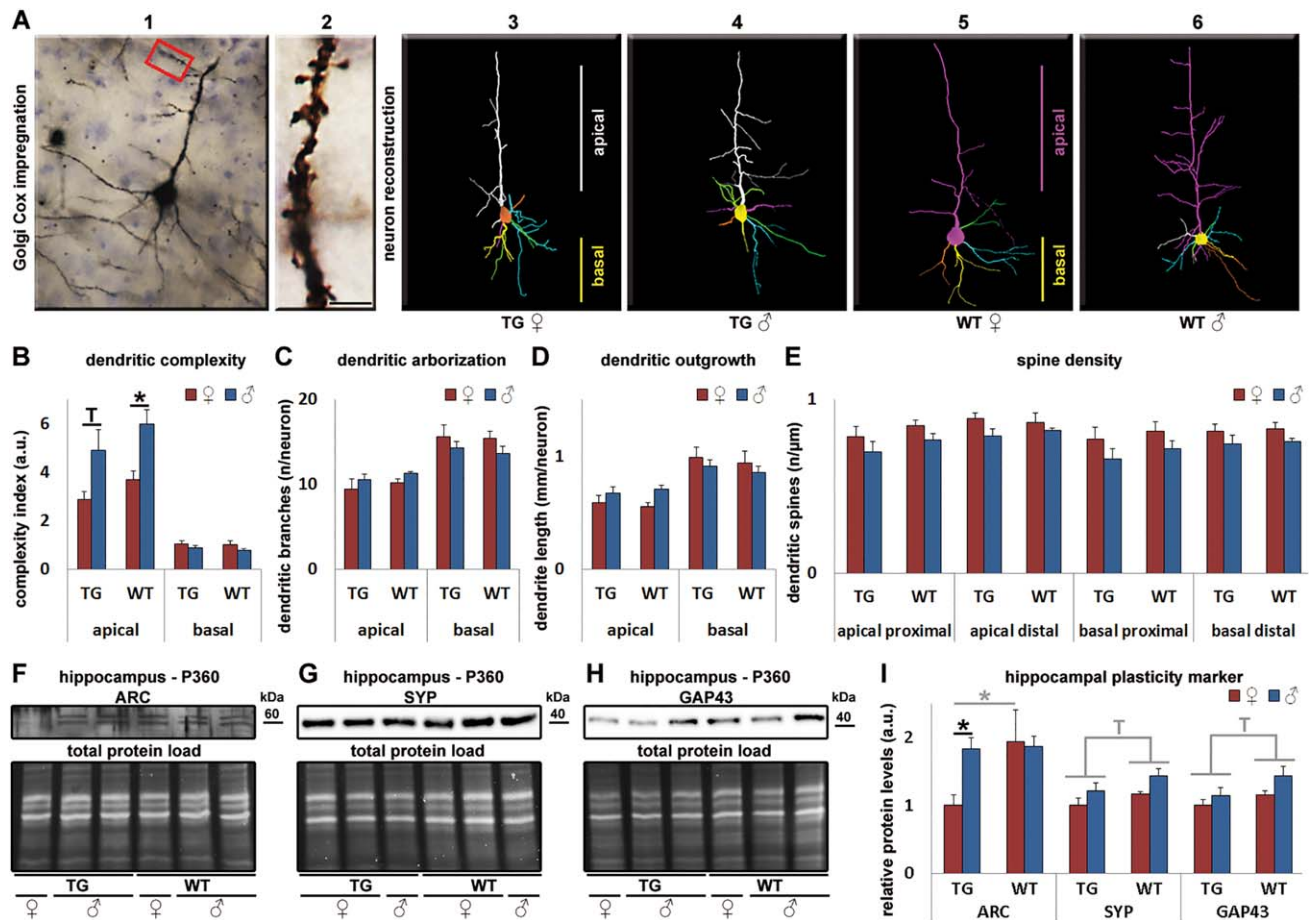
Figure 6. *Structural neuroplasticity is slightly affected in aged female brains.* **A.** Image of a Golgi Cox impregnated, frontal cortex neuron from layer V (image 1) and a magnified dendrite with spines (image 2) from the same neuron (indicated by the red rectangle). Scale bar: 3 μm. Representative images (images 3–6) of digital reconstructions from Golgi Cox stained neurons from P360 days old transgenic (TG) and wildtype (WT) females (♀) and males (♂). The complexity index of apical and basal dendrites (**B**), the number of dendritic branches (**C**) and the dendritic length (**D**) per neuron as well as the dendritic spine density per μm (**E**) were determined in all four murine groups. Hippocampal protein expression of the structural neuroplasticity marker ARC (**F**, **I**), SYP (**G**, I) and GAP43 (**H**, I) in TG and WT females and males. $^{T}0.05 \leq P < 0.01$, $*P < 0.05$ (2-way ANOVA and Bonferroni post hoc test). Black asterisks indicate comparison between female and male groups, gray asterisks indicate comparison between age- and sex-matched TG and WT mice. TG ♀: n = 4–7, TG ♂: n = 5–6, WT: n = 5 per sex. Results are shown as mean ± SEM.

Preexisting reports on the influence of female sex hormones on Alzheimer's pathogenesis are somewhat controversial. While estrogen treatment fails to improve cognition in menopausal women undergoing hormonal replacement therapy (19, 23), it enhances Aβ phagocytosis in human microglia culture (39) and antagonizes Aβ and tau pathology (48) under experimental conditions. For the male sex hormone testosterone however, a protective role against Alzheimer's disease prevails in the pre-existing literature. Testosterone promotes anti-amyloidogenic APP processing and inhibits Aβ production and Aβ induced neurotoxicity *in vitro* (24, 25). It further reduces Aβ levels *in vivo*, possibly through enhanced neprilysin-triggered Aβ degradation, thereby improving cognitive performance (38, 52, 54, 65). With the present study, we provide new pathomechanistic links between estrogen, testosterone and Alzheimer's disease susceptibility. Although estrogen *per se* might possess neuroprotective functions (57) it seems to enhance KLK8 levels, which in turn exerts harmful effects, whereas testosterone

does not influence neuronal or microglial KLK8 synthesis. Additionally, estrogen in comparison to testosterone seems to have a reduced potential to protect microglia from Aβ toxicity and to promote microglial Aβ clearance.

Although the precise mechanisms remain unknown KLK8 excess possibly promotes Alzheimer's pathogenesis by abnormally high processing rates and subsequent depletion of its substrates ephrin receptor B2 (EPHB2) (5), fibronectin (56), neural cell adhesion molecule L1 (L1CAM) (41) and neuregulin-1 (60). A lack of EPHB2 might deteriorate cognitive function (13), affect vessel pathology (1) as well as autophagy (12, 33) whereas depletion of fibronectin, L1CAM and neuregulin-1 could increase Aβ biogenesis (44), plaque precipitation (17) and Aβ-induced neuronal apoptosis (16), respectively. At least for EPHB2 (28) and fibronectin (this study, see Figure 4D,E), reduced levels of unprocessed, full-length substrates could be detected in AD affected brains.
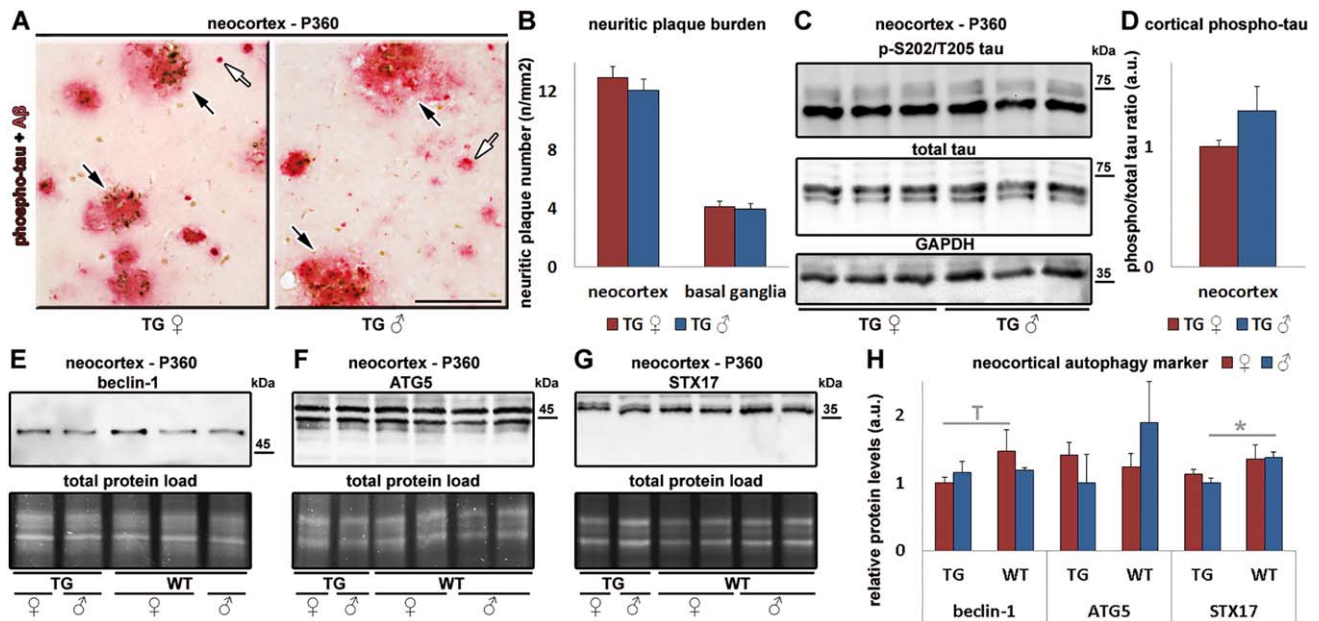
Figure 7. *Female and male brains are equally affected by tau pathology and autophagy impairments.* **A.** Anti-phospho-tau (AT8) and anti-Aβ double immunostaining visualize neuritic, AT8-positive (black arrows) and non-neuritic, AT8-negative (white arrows) Aβ plaques in the neocortex of 1-year-old transgenic (TG) female (♀) and male (♂) mice. Scale bar: 100 μm. **B.** Stereological quantification of the neuritic plaque number in the neocortex and basal ganglia. **C** and **D.** Tau phosphorylation levels at S202/T205 normalized against total tau amounts and GAPDH. Neocortical protein expression of the autophagy marker beclin-1 (**E**, **H**), ATG5 (**F**, H) and STX17 (**G**, **H**) in TG and wild-type (WT) females and males. $^{T}0.05 \leq P < 0.01$, $^{*}P < 0.05$ [2-way ANOVA and Bonferroni post hoc test for multiple-groups comparison as in (H), Student's t-test with Bonferroni correction for two-groups comparison as in (B) and (D)]. Gray asterisks indicate comparison between age- and sex-matched TG and WT mice. TG ♀: n = 7, TG ♂: n = 6, WT: n = 5 per sex. Results are shown as mean ± SEM.

Interestingly, KLK8 excess could be also detected in brains of female non-AD affected patients and female wildtype mice in an advanced age, in mice along with impaired spatial memory performance and reduced dendritic complexity, when compared to males. This finding hints at the possibility of a principal female sex-preference for neurodegeneration during physiological aging.

In summary, we here demonstrate that multiple features of Alzheimer's pathology are more pronounced in female than in male mice and that these sex-specific differences all evolve after the emergence of cerebral KLK8 excess in females. We therefore conclude that KLK8 overexpression might be a causative element for the preferential prevalence of Alzheimer's disease in females.

ACKNOWLEDGMENTS

CONFLICT OF INTEREST

The authors declare that they have no actual or potential conflicts of interest.

REFERENCES

1. Adams RH, Wilkinson GA, Weiss C, Diella F, Gale NW, Deutsch U et al (1999) Roles of ephrinB ligands and EphB receptors in cardiovascular development: demarcation of arterial/venous domains, vascular morphogenesis, and sprouting angiogenesis. *Genes Dev* **13**: 295–306.

2. Altmann A, Tian L, Henderson VW, Greicius MD (2014) Sex modifies the APOE-related risk of developing Alzheimer disease. *Ann Neurol* **75**:563–573.

3. Ambree O, Leimer U, Herring A, Gortz N, Sachser N, Heneka MT et al (2006) Reduction of amyloid angiopathy and Abeta plaque burden after enriched housing in TgCRND8 mice: involvement of multiple pathways. *Am J Pathol* **169**:544–552.

4. Ambree O, Touma C, Gortz N, Keyvani K, Paulus W, Palme R et al (2006) Activity changes and marked stereotypic behavior precede Abeta pathology in TgCRND8 Alzheimer mice. *Neurobiol Aging* **27**: 955–964.

5. Attwood BK, Bourgognon JM, Patel S, Mucha M, Schiavon E, Skrzypiec AE et al (2011) Neuropsin cleaves EphB2 in the amygdala to control anxiety. *Nature* **473**:372–375.

6. Barron AM, Pike CJ (2012) Sex hormones, aging, and Alzheimer's disease. *Front Biosci (Elite Ed)* **4**:976–997.

7. Braak H, Braak E (1991) Neuropathological staging of Alzheimer-related changes. *Acta Neuropathol* **82**:239–259.

8. Brookmeyer R, Evans DA, Hebert L, Langa KM, Heeringa SG, Plassman BL et al (2011) National estimates of the prevalence of Alzheimer's disease in the United States. *Alzheimers Dement* **7**:61–73.

9. Callahan MJ, Lipinski WJ, Bian F, Durham RA, Pack A, Walker LC (2001) Augmented senile plaque load in aged female beta-amyloid precursor protein-transgenic mice. *Am J Pathol* **158**:1173–1177.

10. Castellano JM, Deane R, Gottesdiener AJ, Verghese PB, Stewart FR, West T *et al* (2012) Low-density lipoprotein receptor overexpression enhances the rate of brain-to-blood Abeta clearance in a mouse model of beta-amyloidosis. *Proc Natl Acad Sci USA* **109**:15502–15507.

11. Chishti MA, Yang DS, Janus C, Phinney AL, Horne P, Pearson J *et al* (2001) Early-onset amyloid deposition and cognitive deficits in transgenic mice expressing a double mutant form of amyloid precursor protein 695. *J Biol Chem* **276**:21562–21570.

12. Chukkapalli S, Amessou M, Dilly AK, Dekhil H, Zhao J, Liu Q *et al* (2014) Role of the EphB2 receptor in autophagy, apoptosis and invasion in human breast cancer cells. *Exp Cell Res* **320**:233–246.

13. Cisse M, Halabisky B, Harris J, Devidze N, Dubal DB, Sun B *et al* (2011) Reversing EphB2 depletion rescues cognitive functions in Alzheimer model. *Nature* **469**:47–52.

14. Clinton LK, Billings LM, Green KN, Caccamo A, Ngo J, Oddo S *et al* (2007) Age-dependent sexual dimorphism in cognition and stress response in the 3xTg-AD mice. *Neurobiol Dis* **28**:76–82.

15. Condello C, Yuan P, Grutzendler J (2018) Microglia-mediated neuroprotection, TREM2, and Alzheimer's disease: evidence from optical imaging. *Biol Psychiatry* **83**:377–387.

16. Cui W, Tao J, Wang Z, Ren M, Zhang Y, Sun Y *et al* (2013) Neuregulin1beta1 antagonizes apoptosis via ErbB4-dependent activation of PI3-kinase/Akt in APP/PS1 transgenic mice. *Neurochem Res* **38**:2237–2246.

17. Djogo N, Jakovcevski I, Muller C, Lee HJ, Xu JC, Jakovcevski M *et al* (2013) Adhesion molecule L1 binds to amyloid beta and reduces Alzheimer's disease pathology in mice. *Neurobiol Dis* **56**:104–115.

18. Dubal DB, Broestl L, Worden K (2012) Sex and gonadal hormones in mouse models of Alzheimer's disease: what is relevant to the human condition?. *Biol Sex Differ* **3**:24.

19. Espeland MA, Rapp SR, Shumaker SA, Brunner R, Manson JE, Sherwin BB *et al* (2004) Conjugated equine estrogens and global cognitive function in postmenopausal women: Women's Health Initiative Memory Study. *JAMA* **291**:2959–2968.

20. Farrer LA, Cupples LA, Haines JL, Hyman B, Kukull WA, Mayeux R *et al* (1997) Effects of age, sex, and ethnicity on the association between apolipoprotein E genotype and Alzheimer disease. A meta-analysis. APOE and Alzheimer Disease Meta Analysis Consortium. *JAMA* **278**:1349–1356.

21. Fimia GM, Di Bartolomeo S, Piacentini M, Cecconi F (2011) Unleashing the Ambra1-Beclin 1 complex from dynein chains: Ulk1 sets Ambra1 free to induce autophagy. *Autophagy* **7**:115–117.

22. Ghavami S, Shojaei S, Yeganeh B, Ande SR, Jangamreddy JR, Mehrpour M *et al* (2014) Autophagy and apoptosis dysfunction in neurodegenerative disorders. *Prog Neurobiol* **112**:24–49.

23. Gleason CE, Dowling NM, Wharton W, Manson JE, Miller VM, Atwood CS *et al* (2015) Effects of hormone therapy on cognition and mood in recently postmenopausal women: findings from the randomized, controlled KEEPS-cognitive and affective study. *PLoS Med* **12**:e1001833. discussion e.

24. Goodenough S, Engert S, Behl C (2000) Testosterone stimulates rapid secretory amyloid precursor protein release from rat hypothalamic cells via the activation of the mitogen-activated protein kinase pathway. *Neurosci Lett* **296**:49–52.

25. Gouras GK, Xu H, Gross RS, Greenfield JP, Hai B, Wang R *et al* (2000) Testosterone reduces neuronal secretion of Alzheimer's beta-amyloid peptides. *Proc Natl Acad Sci USA* **97**:1202–1205.

26. Hennessy E, Griffin EW, Cunningham C (2015) Astrocytes are primed by chronic neurodegeneration to produce exaggerated chemokine and cell infiltration responses to acute stimulation with the cytokines IL-1beta and TNF-alpha. *J Neurosci* **35**:8411–8422.

27. Herring A, Donath A, Yarmolenko M, Uslar E, Conzen C, Kanakis D *et al* (2012) Exercise during pregnancy mitigates Alzheimer-like pathology in mouse offspring. *FASEB J* **26**:117–128.

28. Herring A, Munster Y, Akkaya T, Moghaddam S, Deinsberger K, Meyer J *et al* (2016) Kallikrein-8 inhibition attenuates Alzheimer's disease pathology in mice. *Alzheimers Dement* **12**:1273–1287.

29. Herring A, Munster Y, Metzdorf J, Bolczek B, Krussel S, Krieter D *et al* (2016) Late running is not too late against Alzheimer's pathology. *Neurobiol Dis* **94**:44–54.

30. Hirata-Fukae C, Li HF, Hoe HS, Gray AJ, Minami SS, Hamada K *et al* (2008) Females exhibit more extensive amyloid, but not tau, pathology in an Alzheimer transgenic model. *Brain Res* **1216**:92–103.

31. Irvine K, Laws KR, Gale TM, Kondel TK (2012) Greater cognitive deterioration in women than men with Alzheimer's disease: a meta analysis. *J Clin Exp Neuropsychol* **34**:989–998.

32. Itakura E, Kishi-Itakura C, Mizushima N (2012) The hairpin-type tail-anchored SNARE syntaxin 17 targets to autophagosomes for fusion with endosomes/lysosomes. *Cell* **151**:1256–1269.

33. Kandouz M, Haidara K, Zhao J, Brisson ML, Batist G (2010) The EphB2 tumor suppressor induces autophagic cell death via concomitant activation of the ERK1/2 and PI3K pathways. *Cell Cycle* **9**:398–407.

34. Kilic E, ElAli A, Kilic U, Guo Z, Ugur M, Uslu U *et al* (2010) Role of Nogo-A in neuronal survival in the reperfused ischemic brain. *J Cereb Blood Flow Metab* **30**:969–984.

35. King DL, Arendash GW, Crawford F, Sterk T, Menendez J, Mullan MJ (1999) Progressive and gender-dependent cognitive impairment in the APP(SW) transgenic mouse model for Alzheimer's disease. *Behav Brain Res* **103**:145–162.

36. Kishi T, Grass L, Soosaipillai A, Shimizu-Okabe C, Diamandis EP (2003) Human kallikrein 8: immunoassay development and identification in tissue extracts and biological fluids. *Clin Chem* **49**:87–96.

37. Kulnane LS, Lamb BT (2001) Neuropathological characterization of mutant amyloid precursor protein yeast artificial chromosome transgenic mice. *Neurobiol Dis* **8**:982–992.

38. Lee JH, Byun MS, Yi D, Choe YM, Choi HJ, Baek H *et al* (2017) Sex-specific association of sex hormones and gonadotropins, with brain amyloid and hippocampal neurodegeneration. *Neurobiol Aging* **58**:34–40.

39. Li R, Shen Y, Yang LB, Lue LF, Finch C, Rogers J (2000) Estrogen enhances uptake of amyloid beta-protein by microglia derived from the human cortex. *J Neurochem* **75**:1447–1454.

40. Lin KA, Choudhury KR, Rathakrishnan BG, Marks DM, Petrella JR, Doraiswamy PM (2015) Marked gender differences in progression of mild cognitive impairment over 8 years. *Alzheimers Dement (N Y)* **1**: 103–110.

41. Matsumoto-Miyai K, Ninomiya A, Yamasaki H, Tamura H, Nakamura Y, Shiosaka S (2003) NMDA-dependent proteolysis of presynaptic adhesion molecule L1 in the hippocampus by neuropsin. *J Neurosci* **23**:7727–7736.

42. Mielke MM, Vemuri P, Rocca WA (2014) Clinical epidemiology of Alzheimer's disease: assessing sex and gender differences. *Clin Epidemiol* **6**:37–48.

43. Mirra SS, Hart MN, Terry RD (1993) Making the diagnosis of Alzheimer's disease. A primer for practicing pathologists. *Arch Pathol Lab Med* **117**:132–144.

44. Monning U, Sandbrink R, Weidemann A, Banati RB, Masters CL, Beyreuther K (1995) Extracellular matrix influences the biogenesis of amyloid precursor protein in microglial cells. *J Biol Chem* **270**: 7104–7110.

45. Palladino G, Nicolia V, Kovacs GG, Canterini S, Ciraci V, Fuso A *et al* (2017) Sexually dimorphic expression of reelin in the brain of a mouse model of Alzheimer disease. *J Mol Neurosci* **61**:359–367.

46. Pike CJ (2001) Testosterone attenuates beta-amyloid toxicity in cultured hippocampal neurons. *Brain Res* **919**:160–165.

47. Pike CJ (2017) Sex and the development of Alzheimer's disease. *J Neurosci Res* **95**:671–680.

48. Pike CJ, Carroll JC, Rosario ER, Barron AM (2009) Protective actions of sex steroid hormones in Alzheimer's disease. *Front Neuroendocrinol* **30**:239–258.

49. Pistell PJ, Zhu M, Ingram DK (2008) Acquisition of conditioned taste aversion is impaired in the amyloid precursor protein/presenilin 1 mouse model of Alzheimer's disease. *Neuroscience* **152**:594–600.

50. Pyo JO, Yoo SM, Ahn HH, Nah J, Hong SH, Kam TI et al (2013) Overexpression of Atg5 in mice activates autophagy and extends lifespan. *Nat Commun* **4**:2300.

51. Raber J, Wong D, Buttini M, Orth M, Bellosta S, Pitas RE et al (1998) Isoform-specific effects of human apolipoprotein E on brain function revealed in ApoE knockout mice: increased susceptibility of females. *Proc Natl Acad Sci USA* **95**:10914–10919.

52. Ramsden M, Nyborg AC, Murphy MP, Chang L, Stanczyk FZ, Golde TE et al (2004) Androgens modulate beta-amyloid levels in male rat brain. *J Neurochem* **87**:1052–1055.

53. Roberts RO, Geda YE, Knopman DS, Cha RH, Pankratz VS, Boeve BF et al (2012) The incidence of MCI differs by subtype and is higher in men: the Mayo Clinic Study of Aging. *Neurology* **78**:342–351.

54. Rosario ER, Carroll JC, Oddo S, LaFerla FM, Pike CJ (2006) Androgens regulate the development of neuropathology in a triple transgenic mouse model of Alzheimer's disease. *J Neurosci* **26**:13384–13389.

55. Rosario ER, Chang L, Stanczyk FZ, Pike CJ (2004) Age-related testosterone depletion and the development of Alzheimer disease. *JAMA* **292**:1431–1432.

56. Shimizu C, Yoshida S, Shibata M, Kato K, Momota Y, Matsumoto K et al (1998) Characterization of recombinant and brain neuropsin, a plasticity-related serine protease. *J Biol Chem* **273**:11189–11196.

57. Simpkins JW, Yi KD, Yang SH, Dykens JA (2010) Mitochondrial mechanisms of estrogen neuroprotection. *Biochim Biophys Acta* **1800**:1113–1120.

58. Snyder HM, Asthana S, Bain L, Brinton R, Craft S, Dubal DB et al (2016) Sex biology contributions to vulnerability to Alzheimer's disease: a think tank convened by the Women's Alzheimer's Research Initiative. *Alzheimers Dement* **12**:1186–1196.

59. Sunyer B, Patil S, Höger H, Lubec G (2007) Barnes maze, a useful task to assess spatial reference memory in the mice. *Protoc Exch* **390**. http://dx.doi.org/10.1038/nprot.2007.390

60. Tamura H, Kawata M, Hamaguchi S, Ishikawa Y, Shiosaka S (2012) Processing of neuregulin-1 by neuropsin regulates GABAergic neuron to control neural plasticity of the mouse hippocampus. *J Neurosci* **32**:12657–12672.

61. Thies W, Bleiler L (2013) 2013 Alzheimer's disease facts and figures. *Alzheimers Dement* **9**:208–245.

62. Ulland TK, Song WM, Huang SC, Ulrich JD, Sergushichev A, Beatty WL et al (2017) TREM2 maintains microglial metabolic fitness in Alzheimer's disease. *Cell* **170**:649–663 e13.

63. Wang J, Tanila H, Puolivali J, Kadish I, van Groen T (2003) Gender differences in the amount and deposition of amyloidbeta in APPswe and PS1 double transgenic mice. *Neurobiol Dis* **14**:318–327.

64. Yang DS, Stavrides P, Mohan PS, Kaushik S, Kumar A, Ohno M et al (2011) Reversal of autophagy dysfunction in the TgCRND8 mouse model of Alzheimer's disease ameliorates amyloid pathologies and memory deficits. *Brain* **134**:258–277.

65. Yao M, Nguyen TV, Rosario ER, Ramsden M, Pike CJ (2008) Androgens regulate neprilysin expression: role in reducing beta-amyloid levels. *J Neurochem* **105**:2477–2488.

66. Zhang F, Zhong R, Li S, Fu Z, Cheng C, Cai H et al (2017) Acute Hypoxia Induced an Imbalanced M1/M2 Activation of Microglia through NF-kappaB Signaling in Alzheimer's Disease Mice and Wild-Type Littermates. *Front Aging Neurosci* **9**:282.

67. Zhao L, Mao Z, Woody SK, Brinton RD (2016) Sex differences in metabolic aging of the brain: insights into female susceptibility to Alzheimer's disease. *Neurobiol Aging* **42**:69–79.

SUPPORTING INFORMATION

Additional Supporting Information may be found in the online version of this article at the publisher's web-site:

Figure 1. Experimental design for microglial and neuronal *in vitro* treatment with sex-hormones. (A) The microglia cell line BV-2 was seeded at 0 days *in vitro* (DIV0) and allowed to grow until DIV2. At DIV2, microglia were either treated with different concentrations (10 nM, 100 nM, 200 nM or 300 nM) of the female-prevalent sex-hormone β-estradiol (β-E2, highlighted in red), or with equimolar concentrations of the male-prevalent sex-hormone dihydroxy-testosterone (DHT, not convertible to oestrogen, highlighted in blue), or with the sex-hormone diluent ethanol (EtOH, 1%, v/v) as control (not depicted). Forty-eight hours later (DIV4), $A\beta_{42}$ (100 nM, highlighted in green) was added to the medium. Six hours (DIV4 + 6h) or 24 h (DIV5) following incubation with $A\beta_{42}$, supernatant and cells were separately collected to quantify remaining extraglial and intraglial $A\beta_{42}$ concentrations by ELISA, enabling determination of $A\beta$ phagocytosis and breakdown efficacy. Additionally, microglial survival was monitored in equally treated cells by an XTT assay. (B) The neuroblastoma cell line SH-SY5Y was seeded at DIV0 and allowed to differentiate until DIV7. At DIV7, neurons were treated with β-E2 (red) or DHT (blue) (each at a concentration of 10 nM, 100 nM, 200 nM or 300 nM) or with 1% EtOH (control, not depicted) for 7 days until DIV14. At DIV14, kallikrein-8 (KLK8) protein levels were determined in neuronal lysates by Western blotting and neuronal survival was monitored by an XTT assay. (C) BV-2 microglia were treated with β-E2 (red) or DHT (blue) or 1% EtOH from DIV2 until DIV4 in analogy to (A) but without $A\beta_{42}$ incubation. At DIV4, microglial KLK8 protein expression and cell survival were determined as in (B).

Figure 2. Diffuse and core plaques surrounded by microglia. (A) Representative image depicting diffuse (white arrows) and core (black arrows) $A\beta$ plaques (highlighted in brown) following single-immunohistochemistry against $A\beta$. (B) Representative image of a diffuse (white asterisk) and core (black asterisks) $A\beta$ plaques (highlighted in red) surrounded by microglia (highlighted in brown) following double-immunohistochemistry against $A\beta$ and the microglia marker AIF1. Scale bars: 100 μm. **Table S1.** List of AD patients and old controls.